Materialia 5 (2019) 100222

Contents lists available at ScienceDirect

Materialia

journal homepage: www.elsevier.com/locate/mtla

Full Length Article

The elastic-strain energy criterion of phase formation for complex concentrated alloys

Angelo F. Andreoli[a,*], Jiri Orava[a], Peter K. Liaw[b], Hans Weber[a], Marcelo F. de Oliveira[c], Kornelius Nielsch[d,e,f], Ivan Kaban[a]

[a] IFW Dresden, Institute for Complex Materials, Helmholtzstr. 20, 01069 Dresden, Germany
[b] Materials Science and Engineering Department, The University of Tennessee, 414 Ferris Hall, Knoxville, TN 37996, USA
[c] Materials Science and Engineering Department, São Carlos School of Engineering, University of São Paulo, Avenida João Dagnone 1100, CEP 13563-120 São Carlos, SP, Brazil
[d] IFW Dresden, Institute for Metallic Materials, Helmholtzstr. 20, 01069 Dresden, Germany
[e] Institute of Materials Science, Technische Universität Dresden, 01062 Dresden, Germany
[f] Institute of Applied Physics, Technische Universität Dresden, 01062 Dresden, Germany

ARTICLE INFO

Keywords:
Complex concentrated alloys
Solid solutions
Intermetallic phases
Elastic-strain energy
Predicting phase formation

ABSTRACT

An empirical method is developed, based on the calculated theoretical elastic-strain energy, to predict the phase formation and its stability for complex concentrated alloys. The method prediction quality is compared with the traditional empirical rules based on the atomic-size mismatch, enthalpy of mixing, and valence-electron concentration for a database of 235 alloys. The "*elastic-strain energy vs. valence-electron concentration*" criterion shows an improved ability to distinguish between single-phase solid solutions, and mixtures of solid solutions and intermetallic phases when compared to the available empirical rules used to date. The criterion is especially strong for alloys that precipitate the μ phase. The theoretical elastic-strain-energy parameter can be combined with other known parameters, such as those noted above, to establish new criteria which can help predict the design of novel complex concentrated alloys with the on-demand combination of mechanical properties.

1. Introduction

High-entropy alloys (HEAs), with simple single-phase solid-solution (SS) crystalline structures (fcc, bcc and hcp), have attracted a scientific attention [1–3] because of their excellent mechanical properties [4]. HEAs were introduced by Yeh et al. [5–9] in 2004, and they are defined as multi-component alloys with (near)-equiatomic composition containing at least 5 principal elements. The term "high entropy" for these solid-solution-(ss)-type alloys refers to the configurational entropy for an ideal solution, $S_{\mathrm{config}}^{\mathrm{ss,ideal}}$, [10]:

$$S_{\mathrm{config}}^{\mathrm{ss,ideal}} = -nR\sum_{i=1}^{N} c_i \ln c_i, \tag{1}$$

where R is the gas constant, n is the number of total moles, N is the number of components, and c_i is the molar fraction of the component i. Because $S_{\mathrm{config}}^{\mathrm{ss,ideal}}$ generally increases with increasing N, and is highest for equiatomic compositions, it has been assumed that the $S_{\mathrm{config}}^{\mathrm{ss,ideal}}$ is the only parameter responsible for the SS stability [5–9]. The contributions of vibrational, magnetic, and electronic entropies to the total entropy are regarded as negligible. Zhang et al. [11] noted that if $S_{\mathrm{config}}^{\mathrm{ss,ideal}}$ was really the only parameter responsible for the phase stability in HEAs, then this trend would mean that: (i) the higher the number of elements in an alloy the greater the probability to form a SS is; (ii) alloys containing the same number of different elements would have the same probability to form a SS; (iii) the highest probability for equiatomic compositions to form a SS than non-equiatomic alloys with the same number of components. The experimental results [12–14] have shown that the simple stability rule based only on $S_{\mathrm{config}}^{\mathrm{ss,ideal}}$ is not enough to explain the phase formations in HEAs.

A definition of complex concentrated alloys (CCAs) was formulated by Miracle et al. [15]; they aimed at exploring the vast compositional space of multi-principal element alloys [14], and not being limited to SS microstructures or to simple crystal structures. Some CCAs reported to date have shown excellent properties, such as high-temperature mechanical strength [4,16], superior fracture toughness [17], high hardness [4], excellent corrosion resistance [18,19] and good fatigue resistance [20–24], for structural and functional applications competitive with the commercially-established alloys, and CCAs can fill the existing gaps on the materials-property maps, represented, for example, by Ashby maps [25].

* Corresponding author.
E-mail address: a.fernandes.andreoli@ifw-dresden.de (A.F. Andreoli).

https://doi.org/10.1016/j.mtla.2019.100222
Received 18 December 2018; Accepted 23 December 2018
Available online 15 January 2019
2589-1529/© 2019 Acta Materialia Inc. Published by Elsevier Ltd. All rights reserved.

A large number of the constituents in CCAs promotes a new search for theoretical and empirical approaches to predict the phase formation and its stability for the alloys without the need of applying costly and time-consuming experiments and computer simulations. In this paper, a simple approach considering the elastic-strain energy, ΔH_{el}, and the valence-electron concentration, *VEC*, is presented. The criterion can distinguish SS alloys from other possible phases for 235 different CCAs taken from the literature. The criterion is compared with other criteria considering, for example, the atomic-size mismatch, δ, and the enthalpy of mixing, ΔH_{mix}, parameters.

2. Empirical methods for designing the microstructure of HEAs

Otto et al. [26] studied the role of ΔH_{mix} and concluded that it is one of the controlling parameters for the phase precipitation in CCAs, whereas the $S^{ss,ideal}_{config}$ alone is not a good parameter to predict the phase stability. Senkov and Miracle [27] pointed out the importance of the enthalpy of mixing of the intermetallic (IM) phases, ΔH^{IM}_{mix}, competing with the SS phase. The authors state that the conditions to suppress an intermetallic phase and to obtain the SS microstructures are given as:

$$k_1^{cr}(T) > \frac{\Delta H^{IM}_{mix}}{\Delta H^{SS}_{mix}}, \tag{2}$$

where k_1^{cr} is a critical value at a given temperature, T, computed as:

$$k_1^{cr}(T) = \frac{T\Delta S^{ss}}{\left|\Delta H^{ss}_{mix}\right|(1-k_2)} + 1, \tag{3}$$

$$k_2 = \frac{\Delta S^{IM}_{config}}{\Delta S^{ss}_{config}}, \tag{4}$$

where ΔS^{IM}_{config} is the ideal configurational entropy of the intermetallic phase, and ΔS^{IM}_{config} is the configurational entropy of an ideal random solid-solution phase. The plot of $k_1^{cr}(T)$ vs. $(\Delta H^{IM}_{mix}/\Delta H_{mix})$ has been used as the criterion to separate IMs and SS phases in CCAs. The Senkov and Miracle criterion [27] works reasonably well, despite the fact that some IM-containing alloys still overlap with the SS alloys region. Furthermore, the authors do not discuss in detail which intermetallic phases are being predicted correctly, and for which alloys the prediction fails.

Zhang et al. [28,29] studied the relation between ΔH_{mix} (Eq. 5), and the atomic-size mismatch, δ (Eq. 6), and concluded that SSs would typically form when ΔH_{mix} is between −15 and 5 kJ mol^{-1} and δ is between 1 and 6%. The mixing enthalpy of a solution of two elements can be estimated using the Miedema's model [30]. The enthalpy of mixing of an *N*-component solid solution can be estimated as follows:

$$\Delta H_{mix} = \sum_{i,j,i\neq j}^{N} c_i c_j \Omega_{ij}, \tag{5}$$

where $\Omega_{ij} = 4\Delta H^{ij}_{mix}$, c_i and c_j are the atomic fractions of the element i and j, and H^{ij}_{mix} is the enthalpy of mixing of a liquid binary alloy. The atomic-size mismatch is calculated as follows:

$$\delta = 100\sqrt{\sum_{i=1}^{N} c_i\left(1-\frac{r_i}{\bar{r}}\right)^2}, \text{ and } \bar{r} = \sum_{i=1}^{N} c_i r_i, \tag{6}$$

where r_i is the atomic radius of the element i.

Following the Hume-Rothery theory for solid solutions, Guo et al. [12] proposed a criterion for the formation of fcc and bcc crystalline structures based on the valence electron concentration (*VEC*):

$$VEC = \sum_{i=1}^{N} c_i (VEC). \tag{7}$$

According to this criterion, fcc crystalline structures are formed when $VEC \geq 8$, and bcc structures develop for $VEC < 6.7$.

According to López and Alonso [31], one of the contributions to the enthalpy of formation of a metallic substitutional solid solution is the elastic energy due to the atomic-size mismatch between solutes and solvents. As stated by Porter and Easterling [32 p., 24], in systems where δ is considerable, the quasichemical model underestimates the change in the internal energy of mixing because the elastic-strain fields are ignored. The elements volume changes upon mixing, and this introduces a strain-energy term into the overall enthalpy. When the difference in elements size is large enough then the strain contribution prevails over the chemical term, see Porter and Easterling [32] for more details.

Toda-Caraballo and Rivera-Díaz-Del-Castillo [33] introduced two empirical parameters based on the lattice distortion for predicting the phase formation of CCAs: the interatomic spacing mismatch, s_m (%), and the bulk modulus mismatch, K_m (%) (see details in Ref. [33]). The enthalpy of mixing, the parameters $\Omega_T = \frac{T S^{ideal}_{mix}}{|H_{mix}|}$ [34] (this parameter is discussed in detail in Section 4), $\mu_T = T_m/T_{SC}$ [35] (T_m− melting point, T_{SC}− spinodal-decomposition temperature), and χ (the Pauling's electronegativity difference between the constituent elements [36]) were plotted as the function of s_m, and additionally K_m vs. $s_m$was also considered. This method shows a good ability to separate SS from duplex phase alloys (e.g., bcc + fcc), ss + intermetallic phases, and bulk metallic glasses (BMGs), although a more complex methodology was used to achieve these results.

Ye et al. [37] developed a general self-contained geometrical model to compute residual intrinsic strains between different atomic-size elements in CCAs. The model takes into account the atomic size, atomic fraction, and packing efficiency. The authors showed that the phase transition from SS to multi-phase microstructures occurs when the root-mean-square of the residual strain increases above ~5%, i.e., the SS exists under near-zero strain conditions only. However, the methodology is not simple and straightforward, compared with the approach proposed in this paper.

Melnick and Soolshenk [13] argued that the lattice elastic-strain energy, ΔH_{el}, derived from δ, which is inherent to CCAs, should be considered to calculate the Gibbs free energy, G, as:

$$\Delta G = \Delta H_{mix} + \Delta H_{el} - T\Delta S, \tag{8}$$

$$\Delta H_{el} = \sum_{i=1}^{N} c_i B_i \frac{(V_i - V)^2}{2V_i}, \tag{9}$$

$$V = \frac{\sum_{i=1}^{N} c_i B_i V_i}{\sum_{i=1}^{N} c_i B_i}, \tag{10}$$

here, respectively B_i and V_i are the bulk modulus and the atomic volume of the element i. The authors did not investigate the effect of ΔH_{el} on the phase stability. The theoretical calculation predicts zero strain for the same atomic sizes though such real crystals may have strains of other origins. The model presented here is used in order to simplify the ΔH_{el} calculations by considering a volumetric strain to occur in a lattice only. However, it has been recently shown that shear-strain effects cannot be ignored, details are given by Ye et al. [38].

In the present study, the effect of ΔH_{el} on the phase stability of CCAs is studied. The elastic-strain energy is calculated via Eq. (9) for 235 different alloys representing 3d-transitional-metals CCAs, refractory CCAs, non-crystalline CCAs, and BMGs. The local V_i and B_i for solid solutions are considered to be equal to the values for one-component systems. The elastic-strain energies are calculated at room temperature, T_0, because all the phases described in the references are at T_0. However, the phases are likely formed at higher temperatures where diffusion is not limited and therefore metastable phases can be formed [39]. The values of r_i are taken from Miracle and Senkov [1], B_i is taken from Ref. [40]. References. [33,41] are used as the databases for the calculated values of δ, ΔH_{mix} and *VEC*. Then, plots of $\langle \Delta H_{el}$ vs. $\delta\rangle$ – Fig. 2, $\langle \Delta H_{el}$ vs. $\Delta H_{mix}\rangle$ – Fig. 3, $\langle \Delta H_{el}$ vs. $VEC\rangle$ – Fig. 4, $\langle \delta$ vs. $VEC\rangle$– Fig. 5, $\langle \Delta H_{mix}$ vs. $VEC\rangle$ – Fig. S1 in the Supplementary Material, $\langle \delta$ vs. $\Delta H_{mix}\rangle$ – Fig. S2, and $\langle \Delta H_{el}$ vs. ΔH_{mix} vs. $VEC\rangle$ – Fig. S3 are produced to evaluate the ability

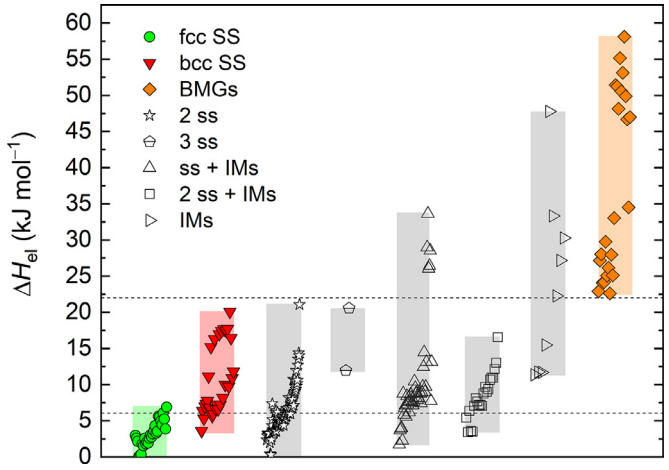

Fig. 1. The elastic-strain energy, ΔH_{el}, parameter for the 235 complex concentrated alloys and bulk metallic glasses (BMGs) given in Table 1 (SS – single-phase solid solution, ss – solid solution, IMs – intermetallics).

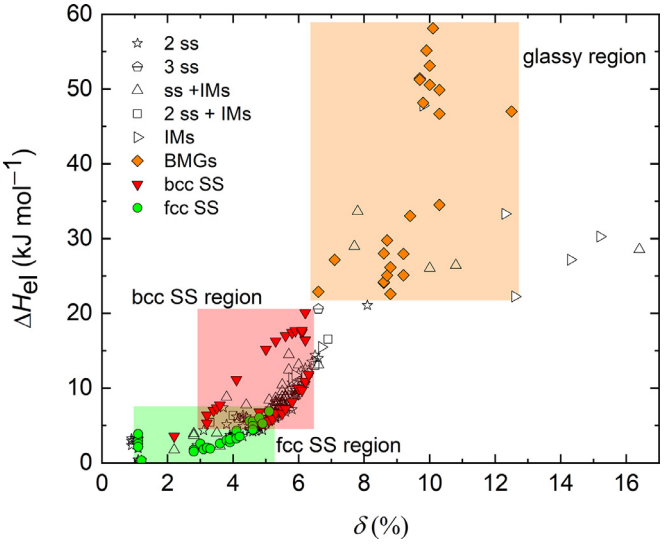

Fig. 2. The $\langle \Delta H_{el}$ vs. $\delta \rangle$ criterion for the 235 complex concentrated alloys and bulk metallic glasses (BMGs) given in Table 1 (SS – single-phase solid solution, ss – solid solution, IMs – intermetallics).

of the different criteria to predict the known microstructures for the 235 alloys. The SS regions, in the above noted plots, are defined as the tangent lines to the outermost SS alloys confined in these areas.

It is to be noted that the early publications on HEAs microstructures relied primarily on X-ray diffraction results, and thus a more detailed description of the phases present could be lacking. However, the extensive database of 235 alloys and the recent publications rely on a combination of techniques to analyze the formed phases.

3. The comparison of different criteria

All the studied 235 CCAs compositions, with the corresponding phases at T_0 taken from the literature, and the calculated values of δ, ΔH_{mix}, *VEC* and ΔH_{el} are shown in Table 1. The $Co_{1.5}CrFeMo_xNi_{1.5}Ti_{0.5}$ ($x = 0$, 0.1, 0.5 and 0.8) alloy family is highlighted in blue in Table 1 and will be discussed separately.

3.1. The ΔH_{el} parameter

The theoretical elastic-strain-energy parameter reveals three characteristic regions for CCAs (Fig. 1). (1) The formation of the fcc SS is mainly in the range of $0 \leq \Delta H_{el} \leq 6.05$ kJ mol^{-1}; the range covers 96.4% of all the fcc SS given in Table 1. The same range of ΔH_{el} contains 4 bcc SS alloys, 46 duplex alloys (fcc + bcc; bcc + fcc; fcc + fcc or bcc + bcc phases, where the first phase is for the matrix and the second phase for the precipitate), and 10 alloys that have a mixture of solid-solution phases and intermetallics. (2) The range of $6.05 < \Delta H_{el} \leq 22$ kJ mol^{-1} describes the bcc SS formation (86.2% of all the bcc SS alloys listed in Table 1), and it is possible to identify duplex alloys, alloys with a mixture of ss and intermetallic phases, and 44% of all the single-phase intermetallic alloys listed in Table 1. (3) For $\Delta H_{el} > 22$ kJ mol^{-1}, all the BMGs and the remaining 56% of the single-phase intermetallic alloys are found.

Seeking to improve the capability to distinguish different phase regions for CCAs, the ΔH_{el} parameter is plotted as the function of the known parameters described in the literature [12,28], and these criteria are discussed in the following subsections. From a designing point of view, it is important to consider not only one parameter to establish reliable predictions of SS regions, but to keep in mind that these parameters may have a synergic effect.

3.2. The $\langle \Delta H_{el}$ vs. $\delta \rangle$ criterion

The criterion is plotted in Fig. 2. All the fcc SS alloys (28 alloys from Table 1) unambiguously lie in the bottom-left region of the plot corresponding to $0 < \Delta H_{el} \leq 6.89$ kJ mol^{-1} and $1.1 \leq \delta \leq 5.1\%$. Please note that these parameters are related via the volume changes in Eqs. (6) and (9). In the same region, 29 alloys with the duplex microstructure are found. This means that for this criterion, 36.2% of all the duplex alloys investigated overlap with the fcc SS region. For the same range of ΔH_{el} and δ, 10 alloys, which have one or more IM phases, are also identified – 13.5% of all the studied alloys that have at least one IM phase (total of 74 alloys containing IM phases are evaluated in Table 1). A different pattern can be noticed for the bcc SS alloys. Eight alloys with the bcc SS microstructure share the same region with the fcc SS alloys. This trend represents 28.6% of the bcc SS alloys listed in Table 1.

The predicted trend in the fcc SS phases formation is consistent with the conclusions [42,43] regarding the phase transition from the fcc to bcc phases for $Al_xCoCrCu_{1-x}FeNiTi_{0.5}$ and $Al_xCoCrFeNi$ alloys. The phase transition occurs due to the decrease in the atomic-packing efficiency and increase in the lattice-distortion energy [44] caused by the addition of the larger Al ($r = 143.17$ pm) than the other constituent elements typical for these alloys. Similar atomic-size effects can be seen when molybdenum content is increased in the $Co_{1.5}CrFeNi_{1.5}Mo_xTi_{0.5}$ ($x = 0$, 0.1, 0.5 and 0.8) alloy (the compositions are highlighted in blue in Table 1). There is a phase transition from the fcc SS for $x = 0.1$ to the fcc + σ phases for $x \geq 0.5$. Except for Ti, Mo has a larger radius ($r = 136.26$ pm) than all the elements that form these alloys. The increasing Mo content rises the lattice distortion, and consequently the elastic-strain energy increases. A closer look at Table 1 shows that varying the Mo concentration does not significantly modify the values of *VEC*, δ and ΔH_{mix} in these alloys. However, ΔH_{el} increased by ~30% ($\Delta H_{el} = 6.05$ kJ mol^{-1} for $x = 0.1$; $\Delta H_{el} = 8.42$ kJ mol^{-1} for $x = 0.5$; and $\Delta H_{el} = 8.66$ kJ mol^{-1} for $x = 0.8$) with the increasing Mo content which favors the transition from fcc SS crystal structure to fcc + σ phases microstructure. It should also be mentioned that the *VEC* of the alloy that forms the SS microstructure is slightly superior to those in which phase separation occurs. The SS alloys sits at the boundary of fcc SSs (see Section 3.4. for detail).

All BMGs lie in the range of $22.6 \leq \Delta H_{el} \leq 58.1$ kJ mol^{-1} and $6.6 \leq \delta \leq 12.5\%$, the latter conforms to the empirical rule for BMGs-formation conditions [45]. Only 7 crystalline alloys overlap with this range: 3 IM alloys (30% of all the alloys with the IM microstructure listed in Table 1) and 4 alloys (6.2%) having a mixture of ss phase(s) and IMs out of the all alloys in Table 1.

The criterion can clearly separate glassy alloys from SS CCAs, and from almost all other phases that form in CCAs. Egami [46,47], and Egami and Waseda [48] discussed that there is a critical value of the

Table 1
The compositions (given mainly in molar fraction, or in at.%[a]), the structures, the microstructures, the atomic-size mismatches (δ), the enthalpies of mixing (ΔH_{mix}), the valence electron concentrations (*VEC*), and the elastic-strain energies (ΔH_{el}) of 235 different complex concentrated alloys.

Composition	Structure	Microstructure	Ref.	δ (%)	ΔH_{mix} (kJ mol^{-1})	*VEC*	ΔH_{el} (kJ mol^{-1})
$Al_{0.25}CoCrCu_{0.75}FeNi$	fcc	fcc SS	[65]	3.1	−0.7	8.4	1.82
$Al_{0.25}CoCrCu_{0.75}FeNiTi_{0.5}$	fcc	fcc SS	[66]	5.1	−7.3	8.0	6.89
$Al_{0.25}CoCrFeMoNi$	fcc + fcc	2ss	[55]	3.7	−7.1	7.8	7.39
$Al_{0.25}CoCrFeNi$	fcc	fcc SS	[67]	3.3	−6.8	7.9	1.91
$Al_{0.25}NbTaTiV$	bcc	bcc SS	[68]	3.5	−4.8	4.6	7.34
$Al_{0.2}CrCuFe$	fcc + bcc	2ss	[12]	2.9	7.7	8.0	2.36
$Al_{0.2}CrCuFeNi_2$	fcc	fcc SS	[12]	2.8	0.1	8.8	1.53
$Al_{0.375}CoCrFeNi$	fcc	fcc SS	[67]	3.9	−8.0	7.8	2.76
$Al_{0.3}CoCrCuFeNi$	fcc	fcc SS	[69]	3.2	0.2	8.5	2.05
$Al_{0.3}CoCrFeMo_{0.1}Ni$	fcc	fcc SS	[55]	3.8	−7.3	7.8	3.04
$Al_{0.3}CoCrFeNi$	fcc + $L1_2$	ss + IM	[55]	3.6	−7.3	7.9	2.26
$Al_{0.3}CoCrFeNiTi_{0.1}$	fcc	fcc SS	[55]	4.1	−8.9	7.8	3.60
$Al_{0.3}CrCuFeMnNi$	fcc + bcc	2ss	[70]	3.1	−0.3	8.1	4.35
$Al_{0.3}CrFe_{1.5}MnNi_{0.5}$	bcc + fcc + B2	2ss + IM	[71]	3.3	−5.5	7.2	5.41
$Al_{0.4}CrCuFeNi_2$	fcc	fcc SS	[12]	3.6	−1.7	8.6	2.60
$Al_{0.5}CoCrCu_{0.5}FeNi$	fcc	fcc SS	[65]	4.1	−4.6	8.0	3.28
$Al_{0.5}CoCrCuFeNiTi$	fcc + bcc + σ	2ss + IM	[72]	6.1	−11.6	7.6	10.97
$Al_{0.5}CoCrCuFeNiTi_{0.2}$	fcc	fcc SS	[72]	4.6	−4.1	8.1	4.96
$Al_{0.5}CoCrCuFeNiTi_{0.4}$	fcc + bcc	2ss	[72]	5.1	−6.4	8.0	6.68
$Al_{0.5}CoCrCuFeNiTi_{0.6}$	fcc + bcc	2ss	[72]	5.5	−8.4	7.9	8.25
$Al_{0.5}CoCrCuFeNiTi_{0.8}$	fcc + bcc + σ	2ss + IM	[72]	5.8	−10.1	7.7	9.67
$Al_{0.5}CoCrCuFeNiTi_{1.2}$	fcc + bcc + σ	2ss + IM	[72]	6.3	−12.9	7.5	12.15
$Al_{0.5}CoCrCuFeNiV$	fcc + bcc + σ	2ss + IM	[73]	4.0	−5.3	7.8	3.57
$Al_{0.5}CoCrCuFeNiV_{0.2}$	fcc	fcc SS	[73]	3.9	−2.5	8.2	3.20
$Al_{0.5}CoCrCuFeNiV_{0.4}$	fcc + bcc	2ss	[73]	3.9	−3.3	8.1	3.32
$Al_{0.5}CoCrCuFeNiV_{0.6}$	fcc + bcc + σ	2ss + IM	[73]	3.9	−4.1	8.0	3.42
$Al_{0.5}CoCrCuFeNiV_{0.8}$	fcc + bcc + σ	2ss + IM	[73]	4.0	−4.7	7.9	3.50
$Al_{0.5}CoCrCuFeNiV_{1.2}$	fcc + bcc	2ss	[73]	4.0	−5.7	7.7	3.54
$Al_{0.5}CoCrCuFeNiV_{1.4}$	fcc + bcc	2ss	[73]	4.0	−6.1	7.6	3.66
$Al_{0.5}CoCrCuFeNiV_{1.6}$	fcc + bcc	2ss	[73]	4.0	−6.5	7.5	3.68
$Al_{0.5}CoCrCuFeNiV_{1.8}$	fcc + bcc	2ss	[73]	3.9	−6.8	7.5	3.72
$Al_{0.5}CoCrCuFeNiV_2$	fcc + bcc	2ss	[73]	3.9	−.1	7.4	3.73
$Al_{0.5}CoCrFeNi$	fcc + bcc	2ss	[67]	4.3	−9.1	7.7	3.54
$Al_{0.5}CoCrFeNiTi$	fcc + bcc + L	2ss + IM	[74]	6.5	−19.6	7.0	13.02
$Al_{0.5}CrCuFeMnNi$	fcc + bcc	2ss	[70]	3.8	−1.9	7.9	5.14
$Al_{0.5}CrFe_{1.5}MnNi_{0.5}$	bcc + fcc + B2	2ss + IM	[71]	4.0	−7.3	7.0	6.36
$Al_{0.5}NbTaTiV$	bcc	bcc SS	[68]	3.4	−8.4	4.6	6.99
$Al_{0.6}CrCuFeNi_2$	fcc	fcc SS	[12]	4.2	−3.3	8.4	3.53
$Al_{0.75}CoCrCu_{0.25}FeNi$	fcc + bcc	2ss	[65]	4.8	−8.5	7.6	4.73
$Al_{0.75}CoCrCu_{0.25}FeNiTi_{0.5}$	bcc + bcc	2ss	[66]	5.9	−14.4	7.3	9.40
$Al_{0.75}CoCrFeNi$	fcc + bcc	2ss	[67]	4.9	−10.9	7.4	4.95
$Al_{0.875}CoCrFeNi$	fcc + bcc	ss + IM	[67]	5.1	−11.7	7.3	5.58
$Al_{0.8}CoCrCuFeNi$	fcc + bcc	2ss	[69]	4.5	−3.6	8.0	4.41
$Al_{0.8}CrCu_{1.5}FeMnNi$	fcc + bcc	2ss	[70]	4.3	−1.7	7.9	4.91
$Al_{0.8}CrCuFe_{1.5}MnNi$	fcc + bcc	2ss	[70]	4.3	−3.3	7.7	5.91
$Al_{0.8}CrCuFeMn_{1.5}Ni$	fcc + bcc	2ss	[70]	4.3	−4.2	7.6	6.39
$Al_{0.8}CrCuFeMnNi$	fcc + bcc	2ss	[70]	4.4	−4.0	7.7	6.19
$Al_{0.8}CrCuFeNi_2$	fcc	fcc SS	[12]	4.6	−4.6	8.2	4.45
$Al_{1.25}CoCrFeNi$	bcc	bcc SS	[67]	5.6	−13.4	7.0	7.24
$Al_{1.2}CrCuFe$	fcc + bcc	2ss	[12]	5.3	−0.5	6.8	8.20
$Al_{1.2}CrCuFeNi_2$	fcc + bcc	2ss	[12]	5.2	−6.8	7.8	6.00
$Al_{1.3}CoCrCuFeNi$	fcc + bcc	2ss	[69]	5.2	−6.2	7.6	6.28
$Al_{1.3}CoCrFeNi$	bcc + B2	ss + IM	[75]	5.7	−13.7	7.0	7.44
$Al_{1.5}CoCrCu_{0.5}FeNi$	fcc + bcc	2ss	[76]	5.6	−10.1	7.2	7.50
$Al_{1.5}CoCrCuFeNi$	fcc + bcc	2ss	[69]	5.4	−7.1	7.5	6.92
$Al_{1.5}CoCrFeNi$	bcc	bcc SS	[67]	5.8	−14.3	6.8	8.17
$Al_{1.6}CoCrCuFeNi$	fcc + fcc + B2	2ss + IM	[72]	5.5	−7.8	7.4	7.22
$Al_{1.75}CoCrFeNi$	bcc + B2	ss + IM	[75]	5.9	−14.9	6.6	8.99
$Al_{1.8}CoCrCuFeNi$	fcc + bcc	2ss	[69]	5.6	−8.1	7.3	7.78
$Al_{10}Cu_{15}Nb_5Ni_{13}Zr_{57}$ [a]	amorphous	BMG	[77]	10.0	−33.9	5.8	50.56
$Al_{10}Cu_{15}Ni_{10}Zr_{65}$ [a]	amorphous	BMG	[78]	9.7	−33.9	5.5	51.43
$Al_{10}Cu_{20}Ni_{12}Ti_5Zr_{53}$ [a]	amorphous	BMG	[78]	10.3	−34.1	6.0	49.87
$Al_{10}Cu_{20}Ni_8Ti_5Zr_{57}$ [a]	amorphous	BMG	[34]	9.8	−31.5	5.8	48.14
$Al_{2.3}CoCrCuFeNi$	fcc + bcc + B2	2ss + IM	[69]	5.9	−9.4	7.0	8.99
$Al_{2.5}CoCrCuFeNi$	fcc + bcc + B2	2ss + IM	[69]	6.0	−9.8	6.9	9.38
$Al_{2.5}CoCrFeNi$	bcc	bcc SS	[79]	6.2	−16.1	6.2	10.90
$Al_{2.8}CoCrCuFeNi$	bcc	bcc SS	[7]	6.0	−10.3	6.7	9.96
$Al_2CoCrCu_{0.5}FeNi$	fcc + bcc	2ss	[8]	5.9	−11.6	6.8	8.95
$Al_2CoCrFeNi$	bcc	bcc SS	[67]	6.1	−15.4	6.5	9.71
$Al_{3.25}CoCrCuFeNi$	fcc + bcc + B2	2ss + IM	[72]	6.1	−10.8	6.5	10.68
$Al_3CoCrFeNi$	bcc	BCC SS	[79]	6.3	−16.4	6.0	11.81
$Al_{7.5}Cu_{17.5}Ni_{10}Zr_{65}$ [a]	amorphous	BMG	[78]	10.0	−32.2	5.8	53.12
$Al_7Cu_{46}Y_5Zr_{42}$ [a]	amorphous	BMG	[80]	12.5	−24.9	7.1	46.99

(*continued on next page*)

Table 1 (*continued*)

Composition	Structure	Microstructure	Ref.	δ (%)	ΔH_{mix} (kJ mol^{-1})	*VEC*	ΔH_{el} (kJ mol^{-1})
$Al_8Cu_{12}Ni_{14}Zr_{66}$ [a]	amorphous	BMG	[78]	9.9	−35.4	5.6	55.15
$Al_8Cu_7Ni_{19}Zr_{66}$ [a]	amorphous	BMG	[78]	10.1	−39.3	5.5	58.12
$Al_9Cu_{16}Ni_9Zr_{66}$ [a]	amorphous	BMG	[78]	9.7	−32.4	5.6	51.23
$AlCo_{0.5}CrCu_{0.5}FeNi$	fcc + bcc	2ss	[76]	5.2	−7.9	7.4	6.18
$AlCo_{0.5}CrCuFeNi$	fcc + bcc	2ss	[81]	5.0	−4.5	7.7	5.64
$AlCo_{0.5}CrFeMo_{0.5}$	bcc + σ	ss + IM	[82]	5.5	−9.7	6.1	10.45
$AlCo_{0.5}CrFeMo_{0.5}Ni$	bcc + σ	ss + IM	[82]	5.6	−11.7	6.9	8.92
$AlCo_{1.5}CrCu_{0.5}FeNi$	fcc + bcc	2ss	[76]	5.0	−7.8	7.7	5.20
$AlCo_{1.5}CrFeMo0.5$	bcc + σ	ss + IM	[82]	5.5	−10.4	6.7	8.79
$AlCo_{1.5}CrFeMo_{0.5}Ni$	bcc + σ	ss + IM	[82]	5.4	−11.1	7.3	7.63
$AlCo_{1.5}CrFeNiTi_{0.5}$	fcc + bcc	2ss	[83]	6.0	−17.2	7.1	9.80
$AlCo_2CrCu_{0.5}FeNi$	fcc + bcc	2ss	[76]	4.8	−7.7	7.8	4.81
$AlCo_2CrFeMo_{0.5}$	fcc + bcc + σ	2ss + IM	[82]	5.4	−10.4	6.9	8.12
$AlCo_2CrFeMo_{0.5}Ni$	fcc + bcc + σ	2ss + IM	[82]	5.3	−10.7	7.4	7.10
$AlCo_2CrFeNiTi_{0.5}$	fcc + bcc	2ss	[83]	5.9	−16.4	7.2	9.09
$AlCo_{3.5}CrCu_{0.5}FeNi$	fcc + bcc	2ss	[76]	4.5	−7.0	8.0	4.50
$AlCo_3CrCu_{0.5}FeNi$	fcc + bcc	2ss	[76]	4.6	−7.3	7.9	4.19
$AlCo_3CrFeNiTi_{0.5}$	fcc + bcc	2ss	[83]	5.7	−15	7.5	7.94
$AlCoCr_{0.5}Cu_{0.5}FeNi$	fcc + bcc	2ss	[76]	5.3	−8.3	7.7	6.17
$AlCoCr_{0.5}CuFeNi$	fcc + bcc	2ss	[81]	5.1	−5.0	8.0	5.64
$AlCoCr_{0.5}FeMo_{0.5}Ni$	bcc + σ	ss + IM	[84]	5.7	−12.1	7.2	8.91
$AlCoCr_{1.5}Cu_{0.5}FeNi$	fcc + bcc	2ss	[76]	4.9	−7.6	7.4	5.21
$AlCoCr_{1.5}FeMo_{0.5}Ni$	bcc + σ	ss + IM	[84]	5.3	−10.8	7.0	7.63
$AlCoCr_2Cu0.5FeNi$	fcc + bcc	2ss	[76]	4.7	−7.2	7.3	4.82
$AlCoCr_2FeMo_{0.5}Ni$	bcc + σ	ss + IM	[84]	5.1	−10.3	6.9	7.12
$AlCoCrCu_{0.25}FeNi$	bcc	bcc SS	[29]	5.2	−9.9	7.4	5.90
$AlCoCrCu_{0.25}FeNiTi_{0.5}$	bcc + bcc	2ss	[85]	6.0	−15.5	7.1	10.15
$AlCoCrCu_{0.5}Fe$	fcc + bcc	2ss	[76]	5.2	−6.1	7.0	6.74
$AlCoCrCu_{0.5}Fe_{0.5}Ni$	fcc + bcc	2ss	[76]	5.3	−8.9	7.5	6.09
$AlCoCrCu_{0.5}Fe_{1.5}Ni$	fcc + bcc	2ss	[76]	4.9	−7.1	7.6	5.80
$AlCoCrCu_{0.5}Fe_2Ni$	fcc + bcc	2ss	[76]	4.7	−6.5	7.6	4.92
$AlCoCrCu_{0.5}FeNi$	bcc	bcc SS	[81]	5.1	−7.9	7.5	5.65
$AlCoCrCu_{0.5}FeNi_{0.5}$	fcc + bcc	2ss	[76]	5.1	−7.3	7.3	6.15
$AlCoCrCu_{0.5}FeNi_{1.5}$	fcc + bcc	2ss	[76]	5.0	−8.3	7.8	5.22
$AlCoCrCu_{0.5}FeNi_2$	fcc + bcc	2ss	[76]	4.9	−8.4	7.9	4.36
$AlCoCrCu_{0.5}FeNi_{2.5}$	fcc + bcc	2ss	[76]	4.8	−8.4	8.1	4.53
$AlCoCrCu_{0.5}FeNi_3$	fcc + bcc	2ss	[76]	4.7	−8.4	8.2	4.25
$AlCoCrCu_{0.5}FeNiTi_{0.5}$	bcc + bcc	2ss	[85]	5.9	−13.4	7.2	9.72
$AlCoCrCu_{0.5}Ni$	bcc	bcc SS	[5]	5.5	−10.2	7.4	6.59
$AlCoCrCuFe_{0.5}Ni$	fcc + bcc	2ss	[81]	5.1	−5.6	7.8	5.56
AlCoCrCuFeMoNiTiVZr	fcc + bcc	2ss	[86]	8.1	−17.2	6.6	21.07
$AlCoCrCuFeNi_{0.5}$	fcc + bcc	2ss	[81]	4.9	−3.9	7.6	5.61
AlCoCrCuFeNiTi	bcc + fcc + bcc	3ss	[87]	6.3	−13.8	7.3	11.95
AlCoCrCuFeNiTiV	fcc + bcc	2ss	[5]	5.9	−13.9	7.0	10.74
AlCoCrCuFeNiV	fcc + bcc	2ss	[87]	4.7	−7.8	7.4	5.21
AlCoCrCuNi	fcc + bcc	2ss	[88]	5.3	−6.6	7.8	5.94
AlCoCrCuNiTi	B2 + fcc + σ	ss + IM	[89]	6.6	−16.7	7.2	13.15
AlCoCrCuNiTiY	$AlNi_2Ti + Cu_2Y$	IM	[89]	15.2	−19.3	6.6	30.26
$AlCoCrCuNiTiY_{0.5}$	$AlNi_2Ti + Cu_2Y$	IM	[89]	12.6	−18.3	6.8	22.26
$AlCoCrCuNiTiY_{0.8}$	$AlNi_2Ti + Cu_2Y$	IM	[89]	14.3	−19.0	6.7	27.17
$AlCoCrFe_{0.6}Mo_{0.5}Ni$	bcc + σ	ss + IM	[90]	5.6	−12.3	7.0	8.75
$AlCoCrFe_{1.5}Mo_{0.5}Ni$	bcc + σ	ss + IM	[90]	5.3	−10.5	7.2	7.73
$AlCoCrFe_2Mo_{0.5}Ni$	bcc + σ	ss + IM	[90]	5.2	−9.7	7.2	7.27
$AlCoCrFeMo_{0.1}Ni$	bcc	bcc SS	[91]	5.3	−12.1	7.2	6.66
$AlCoCrFeMo_{0.2}Ni$	bcc + σ	ss + IM	[91]	5.4	−12.0	7.2	7.12
$AlCoCrFeMo_{0.3}Ni$	bcc + σ	ss + IM	[91]	5.4	−11.8	7.1	7.52
$AlCoCrFeMo_{0.4}Ni$	bcc +σ	ss + IM	[91]	5.5	−11.6	7.1	7.89
$AlCoCrFeMo_{0.5}$	bcc + σ	ss + IM	[82]	5.5	−10.3	6.4	9.56
$AlCoCrFeMo_{0.5}Ni$	bcc + σ	ss + IM	[90]	5.5	−11.4	7.1	8.23
$AlCoCrFeMo_{0.5}Ni_{0.5}$	bcc + σ	ss + IM	[92]	5.5	−11.1	6.8	8.86
$AlCoCrFeMo_{0.5}Ni_{1.5}$	fcc + bcc + σ	2ss + IM	[92]	5.4	−11.5	7.3	7.67
$AlCoCrFeMo_{0.5}Ni_2$	fcc + bcc + σ	2ss + IM	[92]	5.4	−11.5	7.5	7.17
$AlCoCrFeNb_{0.1}Ni$	bcc	bcc SS	[93]	5.5	−13.3	7.2	7.26
$AlCoCrFeNb_{0.25}Ni$	bcc + bcc + L	ss + IM	[93]	5.8	−14.7	7.1	8.77
$AlCoCrFeNb_{0.5}Ni$	fcc + bcc + L	ss + IM	[93]	6.2	−16.5	7.0	10.95
AlCoCrFeNi	fcc + B2	ss + IM	[75]	5.3	−12.3	7.2	6.17
AlCoCrFeNiTi	bcc + bcc	2ss	[94]	6.6	−21.6	6.7	14.00
$AlCoCrFeNiTi_{0.5}$	bcc + bcc	2ss	[83]	6.2	−17.9	6.9	10.62
$AlCoCrFeNiTi_{1.5}$	fcc + bcc + L	2ss + IM	[94]	6.9	−23.9	6.5	16.54
AlCoCrFeNiTiVZr	amorphous	BMG	[78]	8.7	−26.8	6.1	25.06
$AlCoCu_{0.33}FeNi$	fcc + fcc + B2	2ss + IM	[95]	5.5	−9.2	7.9	7.06
$AlCoCu_{0.5}FeNi$	fcc + bcc	2ss	[76]	5.6	−8.7	7.9	6.80
AlCoCuNi	fcc + bcc	2ss	[88]	5.8	−8.0	8.3	7.13
$AlCoFeMo_{0.5}Ni$	bcc + σ	SS + IM	[84]	6.0	−12.7	7.3	9.71
$AlCr_{0.5}CuFeNiTi$	fcc + bcc	2ss	[96]	6.5	−15.4	7.1	14.40

(*continued on next page*)

Table 1 (*continued*)

Composition	Structure	Microstructure	Ref.	δ (%)	ΔH_{mix} (kJ mol^{-1})	*VEC*	ΔH_{el} (kJ mol^{-1})
$AlCr_{1.5}CuFeNiTi$	fcc + bcc	2ss	[96]	6.2	−12.3	6.9	12.69
$AlCr_2CuFeNiTi$	fcc + bcc	2ss	[96]	6.0	−11.1	6.9	11.96
$AlCr_3CuFeNiTi$	fcc + bcc	2ss	[96]	5.8	−9.3	6.8	10.73
$AlCrCu_{0.5}FeNi$	fcc + bcc	2ss	[76]	5.3	−7.7	7.2	6.82
AlCrCuFeMnNi	bcc	bcc SS	[70]	4.8	−5.1	7.5	6.80
$AlCrCuFeNi_2$	fcc	fcc SS	[12]	4.9	−5.8	8.0	5.26
AlCrCuFeNiTi	fcc + bcc	2ss	[96]	6.4	−13.7	7.0	13.51
$AlCrFeNi_{0.75}$	bcc + B2	ss + IM	[95]	5.6	−13.2	6.5	8.11
AlCrMoTaTiZr	amorphous	BMG	[97]	6.6	−16.1	4.7	22.89
AlCrTaTiZr	amorphous	BMG	[98]	7.1	−20.0	4.4	27.16
AlFeNiTiVZr	amorphous	BMG	[78]	8.7	−31.3	5.7	29.75
AlNbTaTiV	bcc	bcc SS	[68]	3.2	−13.4	4.4	6.37
AlTiVYZr	compound	IM	[29]	12.3	−14.9	3.8	33.31
$Co_{1.5}CrFeNi_{1.5}Ti_{0.5}$	fcc	fcc SS	[99]	4.6	−10.7	8.1	5.54
$Co_{1.5}CrFeMo_{0.1}Ni_{1.5}Ti_{0.5}$	fcc	fcc SS	[99]	4.8	−10.6	8.1	6.05
$Co_{1.5}CrFeMo_{0.5}Ni_{1.5}Ti_{0.5}$	fcc + σ	ss + IM	[99]	5.1	−10.3	7.9	8.42
$Co_{1.5}CrFeMo_{0.8}Ni_{1.5}Ti_{0.5}$	fcc + σ	ss + IM	[99]	5.3	−10	7.8	8.66
$CoCrCu_{0.5}FeNi$	fcc	fcc SS	[100]	1.2	0.5	8.6	0.22
$CoCrCu_{0.75}FeNi$	fcc + fcc	2ss	[72]	1.2	2.2	8.7	0.28
CoCrCuFeMn	fcc + bcc	2ss	[26]	0.9	4.2	8.2	2.92
CoCrCuFeMnNi	fcc	fcc SS	[14]	1.1	1.4	8.5	2.57
CoCrCuFeNi	fcc	fcc SS	[101]	1.2	3.2	8.8	0.34
CoCrCuFeNiTi	fcc + L	ss + IM	[101]	5.7	−8.4	8.0	9.73
$CoCrCuFeNiTi_{0.5}$	fcc	fcc SS	[101]	4.5	−3.7	8.4	5.61
$CoCrCuFeNiTi_{0.8}$	fcc + L	ss + IM	[101]	5.3	−6.8	8.1	8.20
$CoCrCuFeNiTi_2$	compound	IM	[29]	6.7	−14.0	7.4	15.48
CoCrCuFeNiTiVZr	amorphous	BMG	[78]	8.8	−16.8	7.1	22.60
CoCrFeMnNbNi	compound	IM	[14]	5.9	−12.0	7.5	11.75
CoCrFeMnNi	fcc	fcc SS	[14]	1.1	−4.2	8.0	2.98
CoCrFeMnNiTi	Compound	IM	[14]	5.8	−13.4	7.3	11.35
$CoCrFeMo_{0.3}Ni$	fcc	fcc SS	[55]	3.0	−4.2	8.1	2.58
$CoCrFeMo_{0.5}Ni$	fcc + σ	ss + IM	[64]	3.5	−4.3	8.0	4.00
$CoCrFeMo_{0.85}Ni$	fcc + σ + μ	ss + IM	[64]	4.2	−4.6	7.9	5.86
CoCrFeMoNiTiVZr	amorphous	BMG	[78]	8.6	−18.8	6.5	24.08
CoCrFeNbNi	fcc + C14	ss + IM	[41]	5.7	−14.9	8.8	12.44
CoCrFeNi	fcc	fcc SS	[100]	1.2	−3.8	8.3	0.03
CoCrFeNiTa	bcc + C14	ss + IM	[41]	5.7	−14.4	8.8	14.48
CoCrFeNiTi	χ + C14 + η	IM	[41]	6.2	−16.3	7.4	11.69
$CoCrFeNiTi_{0.3}$	fcc	fcc SS	[102]	4.1	−8.9	8.0	4.30
$CoCrFeNiTi_{0.5}$	fcc + L + σ + R	ss + IM	[102]	5.0	−11.6	7.8	6.74
CoCrFeNiV	fcc + σ	ss + IM	[41]	2.2	−9.0	8.8	1.74
CoCrFeNiW	fcc + μ	ss + IM	[41]	3.8	−2.9	7.8	8.80
CoCrFeNiY	bcc + Y + YNi + Y_2	ss + IM	[41]	16.4	−9.3	7.2	28.54
CoCrFeNiZr	bcc + C15	ss + IM	[41]	10.8	−22.7	7.4	26.43
CoCrMnNiV	fcc + σ	ss + IM	[26]	2.8	−9.1	7.4	3.68
CoCuFeNi	fcc + fcc	2ss	[95]	1.1	4.7	9.5	0.42
CoCuFeNiTiVZr	amorphous	BMG	[78]	9.2	−20.2	7.3	25.10
CoCuFeNiV	fcc	fcc SS	[29]	2.8	−2.2	8.6	1.78
CoFeMnMoNi	fcc + μ	ss + IM	[26]	4.4	−4.0	8.0	7.74
CoFeMnNiV	fcc + σ	ss + IM	[26]	2.8	−9.0	7.8	3.93
CoFeMoNiTiVZr	amorphous	BMG	[78]	8.8	−21.8	6.6	26.15
$Cr_2Cu_2Fe_2MnNi_2$	fcc + bcc	2ss	[103]	1.1	3.6	8.6	1.95
$Cr_2Cu_2FeMn_2Ni_2$	fcc + bcc	2ss	[103]	1.1	2.4	8.4	3.14
$Cr_2CuFe_2Mn_2Ni_2$	fcc + bcc	2ss	[103]	1.0	0.1	8.1	3.30
Cr_2CuFe_2MnNi	fcc + bcc	2ss	[103]	0.9	2.6	8.0	2.35
$CrCu_{0.7}FeNi$	fcc + bcc	2ss	[104]	1.2	3.0	8.6	0.35
$CrCu_2Fe_2Mn_2Ni$	fcc + bcc	2ss	[103]	0.9	4.7	8.5	3.24
$CrCu_2Fe_2MnNi_2$	fcc	fcc SS	[103]	1.1	3.9	8.9	2.16
$CrCuFeMn_2Ni_2$	fcc	fcc SS	[103]	1.1	−0.5	8.4	3.88
CrCuFeMnNi	fcc + bcc	2ss	[79]	1.0	2.7	8.4	3.00
CrCuFeMoNi	fcc + bcc	2ss	[79]	4.1	4.6	8.2	6.17
CrCuFeNiZr	bcc + IM	ss + IM	[79]	10.0	−14.4	7.8	26.04
CrCuMnNi	fcc + bcc	2ss	[105]	1.1	1.8	8.5	3.26
CrFeMnNiTi	bcc + L	ss + IM	[14]	6.0	−13.3	7.0	13.14
CrNbTiVZr	bcc + IM	ss + IM	[106]	7.7	−4.6	4.8	28.98
CrNbTiZr	bcc + IM	ss + IM	[106]	7.8	−5.0	4.8	33.64
$Cu_{47}Ni_8Ti_{34}Zr_{11}$ [a]	amorphous	BMG	[77]	8.6	−15.4	7.8	24.19
$Cu_{60}Hf_{10}Ti_{10}Zr_{20}$ [a]	amorphous	BMG	[78]	10.3	−17.3	8.2	34.51
CuFeHfTiZr	IM	IM	[107]	9.8	−15.8	6.2	47.77
CuFeNiTiVZr	amorphous	BMG	[78]	9.2	−18.8	7.0	27.95
CuHfNiTiZr	amorphous	BMG	[107]	10.3	−27.4	6.6	46.69
CuNbNiTiZr	amorphous	BMG	[39]	9.4	−21.3	6.8	33.03
FeMoNiTiVZr	amorphous	BMG	[78]	8.6	−19.8	6.2	28.02
HfNbTaTiZr	bcc	bcc SS	[108]	4.1	2.7	4.4	11.13

(*continued on next page*)

Table 1 (*continued*)

Composition	Structure	Microstructure	Ref.	δ (%)	ΔH_{mix} (kJ mol^{-1})	*VEC*	ΔH_{el} (kJ mol^{-1})
MoNbTaVW	bcc	bcc SS	[16]	3.2	−4.6	5.4	5.31
MoNbTaW	bcc	bcc SS	[16]	2.2	−6.5	5.5	3.59
$MoNbTiV_{0.25}Zr$	bcc	bcc SS	[109]	5.3	−2.6	4.8	16.29
$MoNbTiV_{0.5}Zr$	bcc	bcc SS	[109]	5.6	−2.7	4.8	17.00
$MoNbTiV_{0.75}Zr$	bcc	bcc SS	[109]	5.8	−2.7	4.8	17.43
$MoNbTiV_{1.5}Zr$	bcc	bcc SS	[109]	6.1	−2.7	4.8	17.70
$MoNbTiV_2Zr$	bcc	bcc SS	[109]	6.1	−2.7	4.8	17.42
$MoNbTiV_3Zr$	bcc	bcc SS	[109]	6.2	−2.5	4.9	16.43
MoNbTiVZr	bcc	bcc SS	[109]	5.9	−2.7	4.8	17.66
MoNbTiZr	bcc	bcc SS	[109]	5.0	−2.5	4.8	15.19
NbTaTiV	bcc	bcc SS	[68]	3.6	−0.3	4.8	7.74
$NbTiV_2Zr$	bcc + bcc + bcc	3ss	[106]	6.6	−1.3	4.6	20.58
NbTiVZr	bcc	bcc SS	[106]	6.2	−0.3	4.5	20.08

[a] The composition is in at.%.

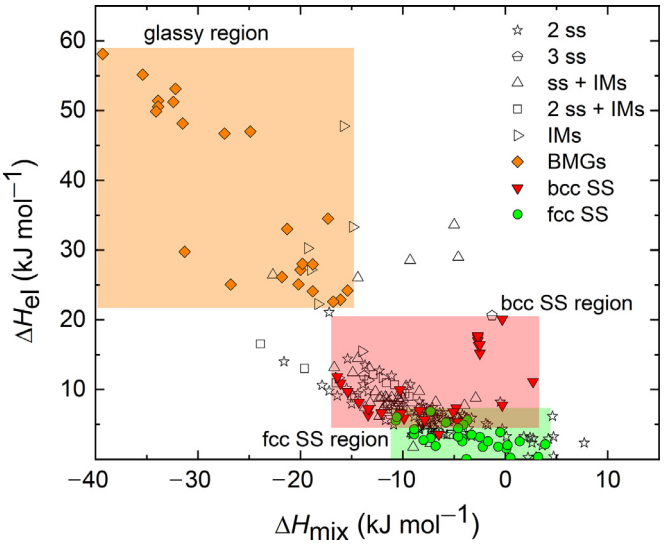

Fig. 3. The $\langle \Delta H_{el}$ vs. $\Delta H_{mix} \rangle$ criterion for the 235 complex concentrated alloys and bulk metallic glasses (BMGs) given in Table 1 (SS – single-phase solid solution, ss – solid solution, IMs – intermetallics).

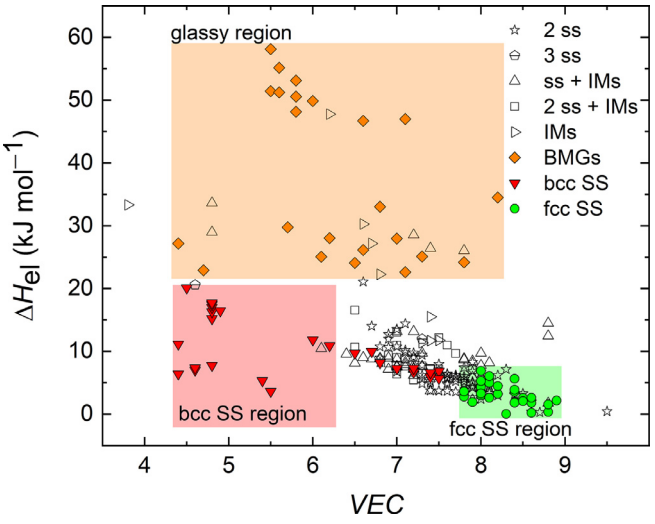

Fig. 4. The $\langle \Delta H_{el}$ vs. *VEC*$\rangle$ criterion for the 235 complex concentrated alloys and bulk metallic glasses (BMGs) given in Table 1 (SS – single-phase solid solution, ss – solid solution, IMs – intermetallics).

volumetric strain, originating from the atomic stresses, where the crystal structure becomes unstable, and consequently it shows a tendency to become non-crystalline. This feature constitutes the local topological instability theory [46]. This concept is sustained by the Hume–Rothery rule that solid solutions are stable when a ratio of the atomic-size difference between solute and solvent atoms is less than 15% for binary alloys.

3.3. *The* $\langle \Delta H_{el}$ *vs.* $\Delta H_{mix} \rangle$ *criterion*

There is a similar pattern for the $\langle \Delta H_{el}$ vs. $\Delta H_{mix} \rangle$ criterion (Fig. 3) to that shown in Fig. 2. The fcc SS populated region lies in the range of $0 < \Delta H_{el} \leq 6.89$ kJ mol^{-1} and $-10.7 \leq \Delta H_{mix} \leq 3.9$ kJ mol^{-1}; the latter condition for the fcc SSs formation was already reported in Zhang and Zhou [28]. The bcc SSs, unlike the fcc SS region, are spread in a broader range of ΔH_{el} and δ, and they overlap with the duplex alloys, IMs, fcc + bcc + IMs, bcc + IMs, and fcc + IMs microstructures. Similarly to the $\langle \Delta H_{el}$ vs. $\delta \rangle$ criterion (Fig. 2), 6 crystalline alloys (5 single-phase IMs and one alloy with a mixture of ss and IM phases) lie in the BMGs region.

The $\langle \Delta H_{el}$ vs. $\Delta H_{mix} \rangle$ criterion, like the $\langle \Delta H_{el}$ vs. $\delta \rangle$ criterion, may work reasonably well to distinguish the fcc SSs within different microstructures, but it clearly cannot separate the bcc ones. The ΔH_{mix} of the bcc SSs studied ranges from −16.4 to 2.7 kJ mol^{-1} (Table 1) which overlaps with the enthalpy of formation for other microstructures, including IMs and BMGs. The criterion may work reasonably well to distinguish the fcc SS region especially for the compositions that tend to ideal solid solutions for the range of $-5 \leq \Delta H_{mix} \leq 5$ kJ mol^{-1}.

From the 22 alloys with the duplex microstructures (fcc + bcc, or fcc + fcc phases) that share the common region with the fcc SS alloys (Fig. 4), 13 have positive values of ΔH_{mix} and all 22 have Cu as the constituent element. Copper is known to have high positive ΔH_{mix} with some transitional metals in binary solutions. This leads to the atoms to organize in A-A and B-B rather than A-B arrangements, and will mostly result in segregation and phase separation. This can explain why these alloys have low values of ΔH_{el} but phase separation occurs. As shown by Otto et al. [26], the phase formation in higher-order multicomponent alloys is consistent with a minimization of the total Gibbs free energy, with contributions of both enthalpy and entropy. They suggest that the binary ΔH_{mix} of the constituent elements will also play an important role in formation of SS or a compound in CCAs.

3.4. *The* $\langle \Delta H_{el}$ *vs.* VEC$\rangle$ *criterion*

The bcc SS populated region is clearly defined in Fig. 4, unlike in Figs., 2 and 3, in the range of $3.59 \leq \Delta H_{el} \leq 20.08$ kJ mol^{-1} and $4.40 \leq$ *VEC* ≤ 6.2. From the 28 CCAs with the bcc SS microstructure in Table 1, 16 (57.1%) lie in this region. In the bcc SS region, 1 alloy containing an IM phase stands, representing 1.3% for these alloys, without any duplex alloys overlap. The remaining bcc SS alloys overlap with other

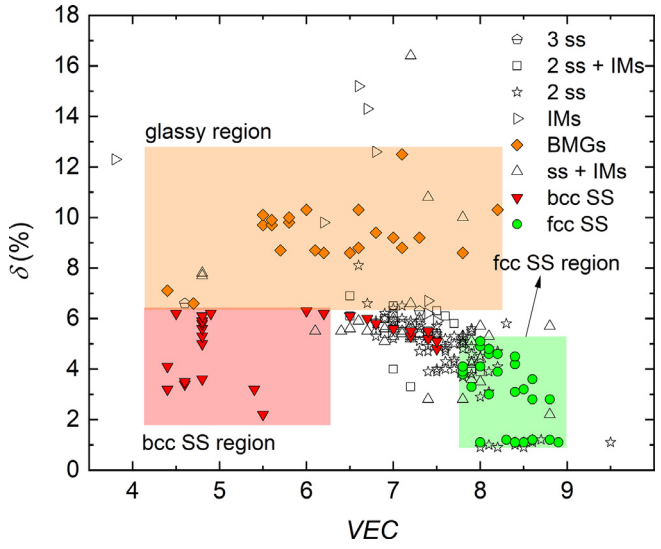

Fig. 5. The ⟨δ vs. *VEC*⟩ criterion for the 235 complex concentrated alloys and bulk metallic glasses (BMGs) given in Table 1 (SS – single-phase solid solution, ss – solid solution, IMs – intermetallics).

microstructures in the range of $6.5 \leq VEC \leq 7.5$. Considering the all 56 SS alloys, including both fcc and bcc alloys, 44 of them fit the limits of ⟨ΔH_{el} vs. *VEC*⟩ for the bcc and fcc SS microstructures. This trend means that 78.6% of all the SS alloys belong to the SS regions highlighted in Fig. 4. In Fig. 4, 22 fcc + bcc, or fcc + fcc alloys (80 alloys from Table 1) duplex microstructures and six alloys containing IM phases (74 in total) overlap with the FCC SS region, yielding 27.5% and 8.1%, respectively. When all microstructures, except of the SS (179 alloys in Table 1), are considered then 16.2% of all these alloys overlap with the SS regions (delimited in Fig. 4). When only the IM-phase-containing alloys are considered then 9.5% overlap with the SS regions is found.

In accordance to what Guo et al. [12] proposed, the *VEC* criterion is able to separate fcc and bcc SSs alloys for CCAs. All the evaluated bcc SS alloys have *VEC* lower than 7.5, while all the fcc SS alloys have *VEC* higher than 7.8. From the 28 alloys with the fcc SS microstructure listed in Table 1, 86% of them obey the range proposed by Guo et al. [12]. For the bcc SS alloys, 79% of them follow the range proposed. The ⟨ΔH_{el} vs. *VEC*⟩ criterion (Fig. 4) shows a plausible ability to distinguish SS alloys from all different microstructures described in the literature for CCAs. The hexagonal-close-packed SSs alloys are not considered in this study because only a few alloys with the hcp SS microstructures have been published [49–53], so far.

It should also be noted that the bcc SS may also form for low values of ΔH_{el}, for example the MoNbTaW and MoNbTaVW alloys have $\Delta H_{el} = 3.59$ kJ mol^{-1} and 5.31 kJ mol^{-1}, respectively. These values are comparable with those for the fcc SS. All the constituent elements of the MoNbTaW and MoNbTaVW alloys have the bcc A2 structure at T_m and T_0. Therefore, it is not surprising that these CCAs precipitate with the same crystal structure characteristic of the constituent elements, in what Miracle and Senkov [1] defined as the "structure in – structure out" correlations (SISO). The SISO analysis takes into account the crystal structure of the element being used to design an alloy, and it develops the Hume–Rothery concept of the link between the crystal structure of an extended SS and the crystal structures of the constituent elements. Therefore, the SISO correlations should also be considered in the CCAs design.

3.5. *The* ⟨δ *vs.* VEC⟩ *criterion*

Two SS regions are distinguishable in Fig. 5 in agreement with the ⟨ΔH_{el} vs. *VEC*⟩ criterion (Fig. 4). In total, 18 alloys with duplex microstructures and 10 IM-containing alloys overlap with the fcc SS region,

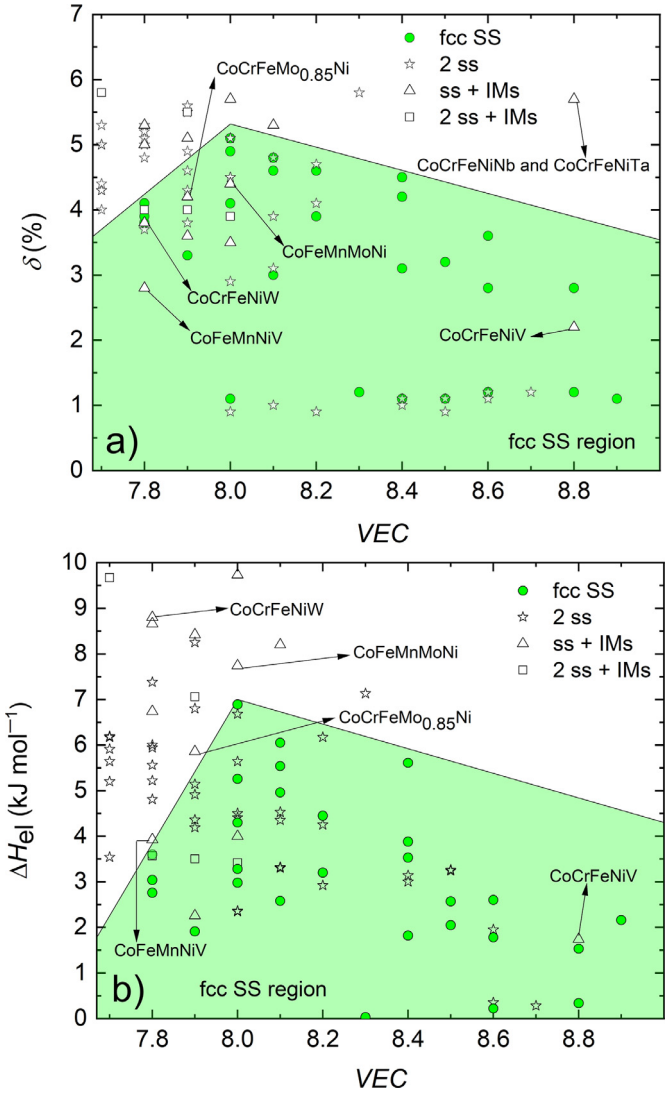

Fig. 6. The ability of two criteria (a) ⟨δ vs. *VEC*⟩ and (b) ⟨ΔH_{el} vs. *VEC*⟩ to correctly predict the phase formation of some intermetallic alloys that overlap with the fcc single-phase solid-solution regions in Figs. 4 and 5, respectively.

which yields 22.5% and 11.5% of these microstructures, respectively. The criterion can correctly predict 40% less in the number of alloys with IM phases than the ⟨ΔH_{el} vs. *VEC*⟩ criterion (Fig. 4). When the bcc SS region is investigated, 1 alloy with a mixture of ss and IM phases and none of the duplex alloys are found. The comparison of the two criteria for the prediction of the fcc SS region is shown for the ⟨δ vs. *VEC*⟩ criterion in Fig. 6a, and for the ⟨ΔH_{el} vs. *VEC*⟩ criterion in Fig. 6b. A clear shift can be seen for some IM-containing alloys to the outside of the fcc SS region in Fig. 6b.

The SS regions can be distinguished in a three-dimensional space considering the electronic, *VEC*, the topological, ΔH_{el}, and the thermodynamic, ΔH_{mix}, parameters by combining Figs. 3 and 4 (see Fig. S3 in the Supplementary Material). For example, the ⟨ΔH_{el} vs. *VEC*⟩ criterion outcomes for the SSs are correct (Fig. 4), in most cases, when the range of $-15 \leq \Delta H_{mix} \leq 5$ kJ mol^{-1}, defined by Zhang et al. [28,29], is satisfied (Fig. 3).

4. Predicting the sigma (σ) and mu (μ) phases

At this point, let us explore the prediction capability of the ΔH_{el} parameter by considering the 6 alloys with a mixture of ss and IM

Table 2
The compositions (in molar fraction), microstructures, and the prediction outcomes using 5 different criteria: $\langle\delta$ vs. $\Delta H_{mix}\rangle$;$\langle\Delta H_{mix}$ vs. VEC$\rangle$;$\langle\Delta H_{el}$ vs. $\Delta H_{mix}\rangle$;$\langle\delta$ vs. VEC$\rangle$; and $\langle\Delta H_{el}$ vs. VEC$\rangle$ for the intermetallic alloys that overlap with the single-phase solid-solution regions for these criteria (L – Laves phase; σ – sigma phase; μ – mu phase).

Composition	Microstructure	Ref.	δ vs. ΔH_{mix}	ΔH_{mix} vs. *VEC*	ΔH_{el} vs. ΔH_{mix}	δ vs. *VEC*	ΔH_{el} vs. *VEC*
			The criterion outcome				
$Al_{0.5}CoCrCuFeNiV$	fcc + bcc + σ	[73]	Failed	Failed	Failed	Failed	Failed
$Al_{0.3}CoCrFeNi$	fcc + $L1_2$	[55]	Failed	Failed	Failed	Failed	Failed
$Al_{0.5}CoCrCuFeNiV_{0.8}$	fcc + bcc + σ	[73]	Failed	Failed	Failed	Failed	Failed
$CoCrFeMo_{0.5}Ni$	fcc + σ	[64]	Failed	Failed	Failed	Failed	Failed
$Al_{0.5}CoCrCuFeNiV_{0.6}$	fcc + bcc + σ	[73]	Failed	Failed	Failed	Failed	Failed
CoCrFeNiV	fcc + σ	[41]	Failed	Failed	Failed	Failed	Failed
CoFeMnNiV	fcc + σ	[26]	Failed	Failed	Failed	Failed	Succeeded
$CoCrFeMo_{0.85}Ni$	fcc + σ + μ	[64]	Failed	Failed	Failed	Failed	Succeeded
CoCrFeNiW	fcc + μ	[41]	Failed	Failed	Succeeded	Failed	Succeeded
CoFeMnMoNi	fcc + μ	[26]	Failed	Failed	Succeeded	Failed	Succeeded
$AlCoCrFe_2Mo_{0.5}Ni$	bcc + σ	[90]	Failed	Succeeded	Failed	Succeeded	Succeeded
$Al_{0.5}CrFe_{1.5}MnNi_{0.5}$	bcc + fcc + B2	[71]	Failed	Succeeded	Failed	Succeeded	Succeeded
$Al_{0.3}CrFe_{1.5}MnNi_{0.5}$	bcc + fcc + B2	[71]	Failed	Succeeded	Failed	Succeeded	Succeeded
CoCrCuFeNiTi	fcc + L	[101]	Succeeded	Failed	Succeeded	Succeeded	Succeeded
$CoCrCuFeNiTi_{0.8}$	fcc + L	[101]	Succeeded	Failed	Succeeded	Succeeded	Succeeded
$Co_{1.5}CrFeMo_{0.8}Ni_{1.5}Ti_{0.5}$	fcc + σ	[99]	Failed	Failed	Succeeded	Succeeded	Succeeded
$AlCoCu_{0.33}FeNi$	fcc + fcc + B2	[95]	Succeeded	Failed	Failed	Succeeded	Succeeded
CoCrMnNiV	fcc + σ	[26]	Failed	Succeeded	Failed	Succeeded	Succeeded

phases that overlap with the fcc SS region delimited in Fig. 4. From these 6 alloys, 5 of them exhibit a mixture of a ss phase, and the sigma, σ, phase usually found in low volume fractions in interdendritic regions and grain boundaries [26]. These 5 alloys are CoCrFeNiV, $CoCrFeMo_{0.5}Ni$, $Al_{0.5}CoCrCuFeNiV$, $Al_{0.5}CoCrCuFeNiV_{0.6}$, and $Al_{0.5}CoCrCuFeNiV_{0.8}$. Four of these alloys contain V, 2 alloys have V as a minor addition, and 2 alloys contain the equimolar concentration. Vanadium is known to extend the σ phase stability in alloys containing Co, Mn and Fe, and it is the only element to form the σ phase, when combined with Ni. "Among the intermetallic phases, it is probably the phase having the broadest range of existence among the different systems" [54]. This seems reasonable to explain why the σ phase forms in these alloys. However, it does not give any insight into how to correctly predict and avoid the precipitation of the σ phase. The remaining $Al_{0.3}CoCrFeNi$ alloy shows a different intermetallic phase – the microstructure is composed of fcc ss and $L1_2$ phase [55].

Table 1 contains 34 alloys with the σ phase. Regarding the elements that are prone to form this phase, 32 alloys contain Cr, 5 alloys contain Ti, 6 alloys contain V, and 23 alloys have Mo. Molybdenum is one of the alloying elements exhibiting the σ phase formation for the largest number of binary systems [54]. Tsai et al. [56] proposed an empirical method using the *VEC* alone to predict the formation range of the σ phase in CCAs. They suggested that alloys were prone to the precipitation of the σ phase when *VEC* is between 6.88 and 7.84, and the method works well for Cr- and V-containing alloys. Eight of the alloys listed in Table 1 (24%), that form the σ phase, fall outside the aforementioned range in *VEC*. All eight alloys contain Cr, 3 of them have V and 5 contain Mo. This suggests that care must be taken when using this criterion to predict SS HEAs, which is demonstrated in Table 2 (the table shows the outcome of different criteria to predict the phase formation for the IM alloys overlapping with the SS regions) and Fig. 6. From the 6 alloys that contain V and form the σ phase, 5 alloys are incorrectly predicted with the $\langle\delta$ vs. *VEC*$\rangle$ criterion (Fig. 6a and Table 2), and 4 alloys are wrongly predicted with the $\langle\Delta H_{el}$ vs. *VEC*$\rangle$ criterion (Fig. 6b and Table 2). It can be concluded that for CCAs of the 3-d transitional metals family, V and Mo may lead (depending on the alloying elements and the overall composition) to the formation of the σ phase, and that the prediction of the σ IM phase for V-containing alloys is somewhat difficult. The reasons for this are discussed in the following paragraphs.

Tsai et al. [41] examined the predicting quality for the phase formation using five different criterion available, with variable terms. The CoCrFeNiX (X = Y, Ti, Zr, Hf, V, Nb, Ta, Cr, Mo, and W) alloys were used as the master composition for the comparison. The empirical methods and the SS-forming conditions are summarized in Table 3. Inclusive of the common rules for ΔH_{mix} (Eq. (5)) [57], δ (Eq. (6)) [57], and Ω_T [34], introduced in Section 2, additional parameters are defined as: [58–60]

$$\omega_L = 1 - \sqrt{\frac{(r_s - \bar{r})^2 - \bar{r}^2}{(r_s + \bar{r})^2}}, \tag{11}$$

$$\omega_S = 1 - \sqrt{\frac{(r_L + \bar{r})^2 - \bar{r}^2}{(r_L + \bar{r})^2}}, \tag{12}$$

$$\gamma = \frac{\omega_S}{\omega_L}, \tag{13}$$

$$\Lambda = \frac{\Delta S_{mix}^{ss,ideal}}{\delta^2}, \tag{14}$$

$$\phi = \frac{S_C - S_H}{S_E}. \tag{15}$$

Here, r_S and r_L are the radii of the smallest and largest atoms in a multicomponent metallic mixture, respectively. The S_C denotes the configurational entropy of mixing for an ideal gas, and the S_E is the excessive entropy of mixing which is the function of atomic packing and atom size. The $S_H = |\Delta H_{mix}|/T_m$ is defined as the complementary entropy. The results by Tsai et al. [41] revealed that 4 criteria, unlike the present work, consistently fail to correctly predict at least the phase formation for the alloys with X = V, Mo, and W; these form the fcc + σ phases for X = V and Mo and fcc + μ phases for the X = W alloy (Table 3). All five methods are unable to correctly predict at least X = V and Mo alloys (Table 3). In the present work, the results show that only for the X = V alloy, it is not possible to separate the fcc SS region using the $\langle\Delta H_{el}$ vs. *VEC*$\rangle$ criterion (Fig. 6b and Table 3). The $\langle\Delta H_{el}$ vs. *VEC*$\rangle$ criterion has greater ability to predict alloys with IM phases, compared with the 5 existing empirical models [41], in particular for alloys that form the μ phase (Table 2). For the σ phase, when Mo is the element leading to its formation, it was also possible to correctly predict the phase formation (Table 1, the alloys highlighted in blue).

Tsai et al. [41] argued that the failure of the well-established methods to correctly predict the regions of the formation of SSs and IMs is because they consider SSs formation only when the ΔH_{mix} is near zero, and δ of the constituent elements is small < 6.6%. However, IM phases can also form with the near-zero mixing enthalpy and for small atomic-size difference. This is the case of the σ and μ phases. One may notice that only the CoCrFeNiV (fcc + σ phases) alloy overlaps with the fcc SS region in Fig. 6b, and 2 alloys overlap with fcc SS region when

Table 3
The single-phase solid-solution (SS) forming conditions and the prediction outcomes for five different approaches, summarized by Tsai et al. [41]. The SS-forming conditions applied to the $\langle \Delta H_{el}$ vs. *VEC*$\rangle$ criterion and the prediction outcomes for the CoCrFeNiX (X = Y, Ti, Zr, Hf, V, Nb, Ta, Cr, Mo and W) alloys.

Model/Ref.	Single-phase solid-solution forming conditions	Incorrect predictions for
Guo et al. [57]	$-11.6 \leq \Delta H_{mix} \leq 3.2$ kJ mol^{-1}; $\delta < 6.6\%$	X = V, Mo and W
Zhang et al. [58]	$-11.6 \leq \Delta H_{mix} \leq 3.2$ kJ mol^{-1}; $\gamma < 1.175$	X = V, Mo and W
Yang et al. [34]	$\Omega \geq 1.1$; $\delta \leq 6.6\%$	X = V, Nb, Ta, Mo and W
Singh et al. [59]	$\Lambda > 0.96$ J K mol^{-1}	X = V and Mo
Ye et al. [60]	$\Phi > 20$	X = V, Mo and W
This work	fcc SS: $0 \leq \Delta H_{el} \leq 6.8$ kJ mol^{-1}; $VEC \geq 8.0$	X = V
This work	bcc SS: $3.59 \leq \Delta H_{el} \leq 20.08$ kJ mol^{-1}; $4.0 \leq VEC \leq 6.2$	—

the atomic-size mismatch criterion is considered in Fig. 6a. These are the CoCrFeNiV and CoCrFeNiW alloys with microstructures of fcc + σ phases and fcc + μ phases, respectively.

The μ phase is a topologically-closed-packed (TCP) phase and has a rhombohedral lattice crystal structure. The phase has been reported for many Ni- and Co-based systems [61–63]. In Table 1, there are 3 alloys that form the μ phase. These are the $CoCrFeMo_{0.85}Ni$ [64], CoCrFeNiW [41], and CoFeMnMoNi [26] alloys (highlighted in green in Table 1). When the $\langle \delta$ vs. *VEC*$\rangle$ criterion is applied, all of the alloys are predicted to be fcc SSs which does not correspond to their real microstructures (Table 2 and Fig. 6a). On the other hand, when the $\langle \Delta H_{el}$ vs. *VEC*$\rangle$ criterion is applied, all three alloys are shifted outside off the fcc SS alloys region (Table 2 and Fig. 6b). It is tempted to assume that the $\langle \delta$ vs. *VEC*$\rangle$ criterion could flawlessly predict the alloys that precipitate the μ phase. However, there are not enough alloys published in the literature to date to fully verify it.

4.1. Comparing the results of ΔH_{el} and δ

The reason that it is possible to correctly predict the formation of the μ phase using ΔH_{el} parameter is that bulk modulus of both Mo and W is typically much higher than for the other constituent elements in these alloys. Therefore, when computing the ΔH_{el}, the bulk modulus has a more pronounced effect contrary to δ. The atomic radii of Mo and W do not differ greatly from the other elements in these alloys. The same applies when predicting alloys that form the σ phase by adding Mo. This can be seen for the highlighted alloys in blue in Table 1. However, when the V-containing alloys forming the σ phase are considered, neither the bulk modulus nor atomic radius of V differs greatly from the other elements. For this reason, both $\langle \delta$ vs. *VEC*$\rangle$ and $\langle \Delta H_{el}$ vs. *VEC*$\rangle$ criteria fail to correctly predict the microstructures despite that the ΔH_{el} parameter has an overall better performance (Table 2).

5. Conclusions

The present study of the extensive database containing 235 complex concentrated alloys reveals clear trends in predicting the phase stability and formation by simple empirical criteria which can be summarized as follows.

1. The ΔH_{el} parameter shows three distinct elastic-strain-energy regions for complex concentrated alloys: (i) the single-phase solid-solution alloys with fcc crystal structure precipitate predominantly in the range of $\Delta H_{el} \leq 6.05$ kJ mol^{-1}; (ii) The range of $6.05 < \Delta H_{el} \leq 22$ kJ mol^{-1} contains most of the bcc SS alloys, and other types of complex concentrated alloys (e.g. ss + IMs, IMs or duplex alloys); and the region (iii) for $\Delta H_{el} > 22$ kJ mol^{-1}, all bulk metallic glasses and ~56% of the single-phase intermetallics can be found.
2. The $\langle \Delta H_{el}$ vs. *VEC*$\rangle$ criterion (Fig. 4) is a simple and straightforward guideline that can be used to predict single-phase solid-solution formation in complex concentrated alloys. The criterion shows an improved ability to predict single-phase solid-solution alloys from intermetallic-forming alloys, especially for the alloys that precipitate the mu μ phase, when it is compared with the different approaches already used in literature.
3. The V-containing complex concentrated alloys forming the sigma σ phase are by far the most common IM phase to overlap within the SS-predicted regions in the literature. The alloys that are prone to form the σ phase and contain V are difficult to predict by using the empirical methods because of their near-zero enthalpy of mixing, low atomic-size mismatch and low elastic-strain energy. Further investigation should be carried out to establish reliable models.
4. The simplified ΔH_{el} parameter improves the quality to predict single-phase solid-solution microstructures compared to the well-established δ parameter. The ΔH_{el} parameter, together with those previously reported in the literature, can be used to design new complex concentrated alloys.

Declaration of interest

None.

Acknowledgments

The present work was conducted during a scholarship supported by the International Cooperation Program CAPES/DAAD/CNPq at the IFW Dresden. The work was financed by CAPES – the Brazilian Federal Agency for Support and Evaluation of Graduate Education (grant number 88887.161381/2017-00, 2017). Peter K. Liaw would like to acknowledge: (i) the Department of Energy (DOE), Office of Fossil Energy, National Energy Technology Laboratory (DE-FE-0011194) with the program manager, Dr. J. Mullen, (ii) the U.S. Army Research Office project (w911NF-13-1-0438) with the programs managers, Drs. M. P. Bakas, S. N. Mashaudhu, and D. M. Stepp and (iii) the support from the National Science Foundation (DMR-1611180 and 1809640) with the program directors, Drs. G. Shiflet and D. Farkas.

Supplementary material

Supplementary material associated with this article can be found, in the online version, at doi:10.1016/j.mtla.2019.100222.

References

[1] D.B. Miracle, O.N. Senkov, A critical review of high entropy alloys and related concepts, Acta Mater. 122 (2017) 448–511, doi:10.1016/j.actamat.2016.08.081.
[2] Y. Zhang, T.T. Zuo, Z. Tang, M.C. Gao, K.A. Dahmen, P.K. Liaw, Z.P. Lu, Microstructures and properties of high-entropy alloys, Prog. Mater. Sci. 61 (2014) 1–93, doi:10.1016/j.pmatsci.2013.10.001.
[3] Z.P. Lu, H. Wang, M.W. Chen, I. Baker, J.W. Yeh, C.T. Liu, T.G. Nieh, An assessment on the future development of high-entropy alloys: summary from a recent workshop, Intermetallics 66 (2015) 67–76, doi:10.1016/j.intermet.2015.06.021.
[4] S. Gorsse, D.B. Miracle, O.N. Senkov, Mapping the world of complex concentrated alloys, Acta Mater. 135 (2017) 177–187, doi:10.1016/j.actamat.2017.06.027.

[5] J.-W. Yeh, S.-J. Lin, T.-S. Chin, J.-Y. Gan, S.-K. Chen, T.-T. Shun, C.-H. Tsau, S.-Y. Chou, Formation of simple crystal structures in Cu-Co-Ni-Cr-Al-Fe-Ti-V alloys with multiprincipal metallic elements, Metall. Mater. Trans. A 35 (2004) 2533–2536, doi:10.1007/s11661-006-0234-4.

[6] Y.Y. Chen, T. Duval, U.D. Hung, J.W. Yeh, H.C. Shih, Microstructure and electrochemical properties of high entropy alloys—a comparison with type-304 stainless steel, Corros. Sci. 47 (2005) 2257–2279, doi:10.1016/j.corsci.2004.11.008.

[7] T.-K. Chen, M.-S. Wong, T.-T. Shun, J.-W. Yeh, Nanostructured nitride films of multi-element high-entropy alloys by reactive DC sputtering, Surf. Coat. Technol. 200 (2005) 1361–1365, doi:10.1016/j.surfcoat.2005.08.081.

[8] C. Hsu, J. Yeh, S. Chen, T. Shun, Wear resistance and high-temperature compression strength of Fcc $CuCoNiCrAl_{0.5}Fe$ alloy with boron addition, Metall. Mater. Trans. A 35 (2004) 1465–1469, doi:10.1007/s11661-004-0254-x.

[9] J.-W. Yeh, Recent progress in high-entropy alloys, Ann. Chim. Sci. Des Matériaux 31 (2006) 633–648, doi:10.3166/acsm.31.633-648.

[10] E.S. Machlin, An Introduction to Aspects of Thermodynamics and Kinetics Relevant to Materials Science, Elsevier, , 2007, doi:10.1016/B978-0-08-046615-6.X5016-4.

[11] F. Zhang, C. Zhang, S.L. Chen, J. Zhu, W.S. Cao, U.R. Kattner, An understanding of high entropy alloys from phase diagram calculations, Calphad 45 (2014) 1–10, doi:10.1016/j.calphad.2013.10.006.

[12] S. Guo, C. Ng, J. Lu, C.T. Liu, Effect of valence electron concentration on stability of fcc or bcc phase in high entropy alloys, J. Appl. Phys. 109 (2011) 103505, doi:10.1063/1.3587228.

[13] A.B. Melnick, V.K. Soolshenko, Thermodynamic design of high-entropy refractory alloys, J. Alloys Compd. 694 (2017) 223–227, doi:10.1016/j.jallcom.2016.09.189.

[14] B. Cantor, I.T.H. Chang, P. Knight, A.J.B. Vincent, Microstructural development in equiatomic multicomponent alloys, Mater. Sci. Eng. A 375–377 (2004) 213–218, doi:10.1016/j.msea.2003.10.257.

[15] D. Miracle, J. Miller, O. Senkov, C. Woodward, M. Uchic, J. Tiley, Exploration and development of high entropy alloys for structural applications, Entropy 16 (2014) 494–525, doi:10.3390/e16010494.

[16] O.N. Senkov, G.B. Wilks, D.B. Miracle, C.P. Chuang, P.K. Liaw, Refractory high-entropy alloys, Intermetallics 18 (2010) 1758–1765, doi:10.1016/j.intermet.2010.05.014.

[17] B. Gludovatz, A. Hohenwarter, D. Catoor, E.H. Chang, E.P. George, R.O. Ritchie, A fracture-resistant high-entropy alloy for cryogenic applications, Science 345 (2014) 1153–1158, doi:10.1126/science.1254581.

[18] Y. Shi, B. Yang, P. Liaw, Corrosion-resistant high-entropy alloys: A review, Metals (Basel) 7 (2017) 43, doi:10.3390/met7020043.

[19] Y. Qiu, M.A. Gibson, H.L. Fraser, N. Birbilis, Corrosion characteristics of high entropy alloys, Mater. Sci. Technol. 31 (2015) 1235–1243, doi:10.1179/1743284715Y.0000000026.

[20] M.A. Hemphill, T. Yuan, G.Y. Wang, J.W. Yeh, C.W. Tsai, A. Chuang, P.K. Liaw, Fatigue behavior of $Al_{0.5}CoCrCuFeNi$ high entropy alloys, Acta Mater. 60 (2012) 5723–5734, doi:10.1016/j.actamat.2012.06.046.

[21] M. Seifi, D. Li, Z. Yong, P.K. Liaw, J.J. Lewandowski, Fracture toughness and fatigue crack growth behavior of as-cast high-entropy alloys, JOM 67 (2015) 2288–2295, doi:10.1007/s11837-015-1563-9.

[22] Z. Tang, T. Yuan, C.-W. Tsai, J.-W. Yeh, C.D. Lundin, P.K. Liaw, Fatigue behavior of a wrought $Al_{0.5}CoCrCuFeNi$ two-phase high-entropy alloy, Acta Mater. 99 (2015) 247–258, doi:10.1016/j.actamat.2015.07.004.

[23] K.V.S. Thurston, B. Gludovatz, A. Hohenwarter, G. Laplanche, E.P. George, R.O. Ritchie, Effect of temperature on the fatigue-crack growth behavior of the high-entropy alloy CrMnFeCoNi, Intermetallics 88 (2017) 65–72, doi:10.1016/j.intermet.2017.05.009.

[24] P. Chen, C. Lee, S.-Y. Wang, M. Seifi, J.J. Lewandowski, K.A. Dahmen, H. Jia, X. Xie, B. Chen, J.-W. Yeh, C.-W. Tsai, T. Yuan, P.K. Liaw, Fatigue behavior of high-entropy alloys: a review, Sci. China Technol. Sci. 61 (2018) 168–178, doi:10.1007/s11431-017-9137-4.

[25] M.F. Ashby, Materials selection in mechanical design, Design (2005), doi:10.1016/B978-1-85617-663-7.00011-4.

[26] F. Otto, Y. Yang, H. Bei, E.P. George, Relative effects of enthalpy and entropy on the phase stability of equiatomic high-entropy alloys, Acta Mater. 61 (2013) 2628–2638, doi:10.1016/j.actamat.2013.01.042.

[27] O.N. Senkov, D.B. Miracle, A new thermodynamic parameter to predict formation of solid solution or intermetallic phases in high entropy alloys, J. Alloys Compd. 658 (2016) 603–607, doi:10.1016/j.jallcom.2015.10.279.

[28] Y. Zhang, Y.J. Zhou, Solid solution formation criteria for high entropy alloys, Mater. Sci. Forum 561–565 (2007) 1337–1339, doi:10.4028/www.scientific.net/MSF.561-565.1337.

[29] Y. Zhang, Y.J. Zhou, J.P. Lin, G.L. Chen, P.K. Liaw, Solid-solution phase formation rules for multi-component alloys, Adv. Eng. Mater. 10 (2008) 534–538, doi:10.1002/adem.200700240.

[30] A. Takeuchi, A. Inoue, Mixing enthalpy of liquid phase calculated by Miedema's scheme and approximated with sub-regular solution model for assessing forming ability of amorphous and glassy alloys, Intermetallics 18 (2010) 1779–1789, doi:10.1016/j.intermet.2010.06.003.

[31] J.M. López, J.A. Alonso, The atomic size-mismatch contribution to the enthalpy of formation of concentrated substitutional metallic solid solutions, Phys. Status Solidi 85 (1984) 423–428, doi:10.1002/pssa.2210850211.

[32] D.A. Porter, K.E. Easterling, Phase Transformations in Metals and Alloys, third ed., CRC Press, 2014, doi:10.1146/annurev.ms.03.080173.001551.

[33] I. Toda-Caraballo, P.E.J. Rivera-Díaz-del-Castillo, A criterion for the formation of high entropy alloys based on lattice distortion, Intermetallics 71 (2016) 76–87, doi:10.1016/j.intermet.2015.12.011.

[34] X. Yang, Y. Zhang, Prediction of high-entropy stabilized solid-solution in multi-component alloys, Mater. Chem. Phys. 132 (2012) 233–238, doi:10.1016/j.matchemphys.2011.11.021.

[35] M.G. Poletti, L. Battezzati, Electronic and thermodynamic criteria for the occurrence of high entropy alloys in metallic systems, Acta Mater. 75 (2014) 297–306, doi:10.1016/j.actamat.2014.04.033.

[36] S. Fang, X. Xiao, L. Xia, W. Li, Y. Dong, Relationship between the widths of supercooled liquid regions and bond parameters of Mg-based bulk metallic glasses, J. Non. Cryst. Solids 321 (2003) 120–125, doi:10.1016/S0022-3093(03)00155-8.

[37] Y.F. Ye, C.T. Liu, Y. Yang, A geometric model for intrinsic residual strain and phase stability in high entropy alloys, Acta Mater. 94 (2015) 152–161, doi:10.1016/j.actamat.2015.04.051.

[38] Y.F. Ye, Y.H. Zhang, Q.F. He, Y. Zhuang, S. Wang, S.Q. Shi, A. Hu, J. Fan, Y. Yang, Atomic-scale distorted lattice in chemically disordered equimolar complex alloys, Acta Mater. 150 (2018) 182–194, doi:10.1016/j.actamat.2018.03.008.

[39] A. Cunliffe, J. Plummer, I. Figueroa, I. Todd, Glass formation in a high entropy alloy system by design, Intermetallics 23 (2012) 204–207, doi:10.1016/j.intermet.2011.12.006.

[40] The photographic periodic table of the elements, Acessed on 12/06/2018. http://periodictable.com/index.html.

[41] M.-H. Tsai, J.-H. Li, A.-C. Fan, P.-H. Tsai, Incorrect predictions of simple solid solution high entropy alloys: cause and possible solution, Scr. Mater. 127 (2017) 6–9, doi:10.1016/j.scriptamat.2016.08.024.

[42] J.Y. He, W.H. Liu, H. Wang, Y. Wu, X.J. Liu, T.G. Nieh, Z.P. Lu, Effects of Al addition on structural evolution and tensile properties of the FeCoNiCrMn high-entropy alloy system, Acta Mater. 62 (2014) 105–113, doi:10.1016/j.actamat.2013.09.037.

[43] Y. Ma, B. Jiang, C. Li, Q. Wang, C. Dong, P. Liaw, F. Xu, L. Sun, The BCC/B2 morphologies in $Al_xNiCoFeCr$ high-entropy alloys, Metals (Basel) 7 (2017) 57, doi:10.3390/met7020057.

[44] J. Li, Q. Fang, B. Liu, Y. Liu, Transformation induced softening and plasticity in high entropy alloys, Acta Mater. 147 (2018) 35–41, doi:10.1016/j.actamat.2018.01.002.

[45] A. Inoue, Stabilization of metallic supercooled liquid and bulk amorphous alloys, Acta Mater. 48 (2000) 279–306, doi:10.1016/S1359-6454(99)00300-6.

[46] T. Egami, Universal criterion for metallic glass formation, Mater. Sci. Eng. A 226–228 (1997) 261–267, doi:10.1016/S0921-5093(97)80041-X.

[47] T. Egami, Atomic level stresses, Prog. Mater. Sci. 56 (2011) 637–653, doi:10.1016/j.pmatsci.2011.01.004.

[48] T. Egami, Y. Waseda, Atomic size effect on the formability of metallic glasses, J. Non. Cryst. Solids 64 (1984) 113–134, doi:10.1016/0022-3093(84)90210-2.

[49] A. Takeuchi, K. Amiya, T. Wada, K. Yubuta, W. Zhang, High-entropy alloys with a hexagonal close-packed structure designed by equi-atomic alloy strategy and binary phase diagrams, JOM 66 (2014) 1984–1992, doi:10.1007/s11837-014-1085-x.

[50] J.O.A. Paschoal, H. Kleykamp, F. Thuemmler, Phase equilibria in the quaternary molybdenum-ruthenium-rhodium-palladium system, Chem. Inf. 15 (1984) 652–664, doi:10.1002/chin.198401016.

[51] C.L. Tracy, S. Park, D.R. Rittman, S.J. Zinkle, H. Bei, M. Lang, R.C. Ewing, W.L. Mao, High pressure synthesis of a hexagonal close-packed phase of the high-entropy alloy CrMnFeCoNi, Nat. Commun. 8 (2017) 15634, doi:10.1038/ncomms15634.

[52] R. Soler, A. Evirgen, M. Yao, C. Kirchlechner, F. Stein, M. Feuerbacher, D. Raabe, G. Dehm, Microstructural and mechanical characterization of an equiatomic YGdTbDyHo high entropy alloy with hexagonal close-packed structure, Acta Mater. 156 (2018) 86–96, doi:10.1016/j.actamat.2018.06.010.

[53] Y.J. Zhao, J.W. Qiao, S.G. Ma, M.C. Gao, H.J. Yang, M.W. Chen, Y. Zhang, A hexagonal close-packed high-entropy alloy: the effect of entropy, Mater. Des. 96 (2016) 10–15, doi:10.1016/j.matdes.2016.01.149.

[54] J.-M. Joubert, Crystal chemistry and Calphad modeling of the σ phase, Prog. Mater. Sci. 53 (2008) 528–583, doi:10.1016/j.pmatsci.2007.04.001.

[55] T.-T. Shun, C.-H. Hung, C.-F. Lee, Formation of ordered/disordered nanoparticles in FCC high entropy alloys, J. Alloys Compd. 493 (2010) 105–109, doi:10.1016/j.jallcom.2009.12.071.

[56] M.-H. Tsai, K.-Y. Tsai, C.-W. Tsai, C. Lee, C.-C. Juan, J.-W. Yeh, Criterion for sigma phase formation in Cr- and V-containing high-entropy alloys, Mater. Res. Lett. 1 (2013) 207–212, doi:10.1080/21663831.2013.831382.

[57] S. Guo, Q. Hu, C. Ng, C.T. Liu, More than entropy in high-entropy alloys: Forming solid solutions or amorphous phase, Intermetallics 41 (2013) 96–103, doi:10.1016/j.intermet.2013.05.002.

[58] Z. Wang, Y. Huang, Y. Yang, J. Wang, C.T. Liu, Atomic-size effect and solid solubility of multicomponent alloys, Scr. Mater. 94 (2015) 28–31, doi:10.1016/j.scriptamat.2014.09.010.

[59] A.K. Singh, N. Kumar, A. Dwivedi, A. Subramaniam, A geometrical parameter for the formation of disordered solid solutions in multi-component alloys, Intermetallics 53 (2014) 112–119, doi:10.1016/j.intermet.2014.04.019.

[60] Y.F. Ye, Q. Wang, J. Lu, C.T. Liu, Y. Yang, Design of high entropy alloys: A single-parameter thermodynamic rule, Scr. Mater. 104 (2015) 53–55, doi:10.1016/j.scriptamat.2015.03.023.

[61] R. Darolia, D. Lahrman, R. Field, Formation of topologically closed packed phases in nickel base single crystal superalloys, in: Proceedings of the Superalloys 1988 (Sixth Int. Symp., TMS), 1988, pp. 255–264, doi:10.7449/1988/Superalloys_1988_255_264.

[62] K. Zhao, Y.H. Ma, L.H. Lou, Z.Q. Hu, μ phase in a nickel base directionally solidified alloy solidified alloy, Mater. Trans. 46 (2005) 54–58, doi:10.2320/matertrans.46.54.

[63] A.S. Wilson, Formation and effect of topologically close-packed phases in nickel-base superalloys, Mater. Sci. Technol. (2017) (United Kingdom), doi:10.1080/02670836.2016.1187335.

[64] T.-T. Shun, L.-Y. Chang, M.-H. Shiu, Microstructure and mechanical properties of multiprincipal component CoCrFeNiMo$_x$ alloys, Mater. Charact. 70 (2012) 63–67, doi:10.1016/j.matchar.2012.05.005.

[65] Y.J. Zhou, Y. Zhang, F.J. Wang, G.L. Chen, Phase transformation induced by lattice distortion in multiprincipal component CoCrFeNiCu$_x$Al$_{1-x}$ solid-solution alloys, Appl. Phys. Lett. 92 (2008) 241917, doi:10.1063/1.2938690.

[66] F.J. Wang, Y. Zhang, G.L. Chen, Atomic packing efficiency and phase transition in a high entropy alloy, J. Alloys Compd. 478 (2009) 321–324, doi:10.1016/j.jallcom.2008.11.059.

[67] H.-P. Chou, Y.-S. Chang, S.-K. Chen, J.-W. Yeh, Microstructure, thermophysical and electrical properties in Al$_x$CoCrFeNi (0≤x≤2) high-entropy alloys, Mater. Sci. Eng. B 163 (2009) 184–189, doi:10.1016/j.mseb.2009.05.024.

[68] X. Yang, Y. Zhang, P.K. Liaw, Microstructure and compressive properties of NbTiVTaAl$_x$ high entropy alloys, Proc. Eng. 36 (2012) 292–298, doi:10.1016/j.proeng.2012.03.043.

[69] J.-W. Yeh, S.-K. Chen, S.-J. Lin, J.-Y. Gan, T.-S. Chin, T.-T. Shun, C.-H. Tsau, S.-Y. Chang, Nanostructured high-entropy alloys with multiple principal elements: Novel alloy design concepts and outcomes, Adv. Eng. Mater. 6 (2004) 299–303, doi:10.1002/adem.200300567.

[70] H.-Y. Chen, C.-W. Tsai, C.-C. Tung, J.-W. Yeh, T.-T. Shun, C.-C. Yang, S.-K. Chen, Effect of the substitution of Co by Mn in Al-Cr-Cu-Fe-Co-Ni high-entropy alloys, Ann. Chim. Sci. Des Matériaux 31 (2006) 685–698, doi:10.3166/acsm.31.685-698.

[71] K.-C. Hsieh, C.-F. Yu, W.-T. Hsieh, W.-R. Chiang, J.S. Ku, J.-H. Lai, C.-P. Tu, C.C. Yang, The microstructure and phase equilibrium of new high performance high-entropy alloys, J. Alloys Compd. 483 (2009) 209–212, doi:10.1016/j.jallcom.2008.08.118.

[72] C.-J. Tong, Y.-L. Chen, J.-W. Yeh, S.-J. Lin, S.-K. Chen, T.-T. Shun, C.-H. Tsau, S.-Y. Chang, Microstructure characterization of Al$_x$CoCrCuFeNi high-entropy alloy system with multiprincipal elements, Metall. Mater. Trans. A 36 (2005) 881–893, doi:10.1007/s11661-005-0283-0.

[73] M.-R. Chen, S.-J. Lin, J.-W. Yeh, M.-H. Chuang, S.-K. Chen, Y.-S. Huang, Effect of vanadium addition on the microstructure, hardness, and wear resistance of Al$_{0.5}$CoCrCuFeNi high-entropy alloy, Metall. Mater. Trans. A 37 (2006) 1363–1369, doi:10.1007/s11661-006-0081-3.

[74] K. Zhang, Z. Fu, Effects of annealing treatment on phase composition and microstructure of CoCrFeNiTiAl$_x$ high-entropy alloys, Intermetallics 22 (2012) 24–32, doi:10.1016/j.intermet.2011.10.010.

[75] Y.-F. Kao, T.-J. Chen, S.-K. Chen, J.-W. Yeh, Microstructure and mechanical property of as-cast, -homogenized, and -deformed Al$_x$CoCrFeNi (0≤x≤2) high-entropy alloys, J. Alloys Compd. 488 (2009) 57–64, doi:10.1016/j.jallcom.2009.08.090.

[76] G.-Y. Ke, G.-Y. Chen, T. Hsu, J.-W. Yeh, FCC and BCC equivalents in as-cast solid solutions of Al$_x$Co$_y$Cr$_z$Cu$_{0.5}$Fe, Ni w high-entropy alloys, Ann. Chim. Sci. Des Matériaux 31 (2006) 669–684, doi:10.3166/acsm.31.669-684.

[77] S. Guo, C.T. Liu, Phase stability in high entropy alloys: Formation of solid-solution phase or amorphous phase, Prog. Nat. Sci. Mater. Int. 21 (2011) 433–446, doi:10.1016/S1002-0071(12)60080-X.

[78] M. Michael, P.K. Liaw, Bulk Metallic Glasses: an Overview, Springer, 2008.

[79] C. Li, J.C. Li, M. Zhao, Q. Jiang, Effect of alloying elements on microstructure and properties of multiprincipal elements high-entropy alloys, J. Alloys Compd. 475 (2009) 752–757, doi:10.1016/j.jallcom.2008.07.124.

[80] Y. Li, S.J. Poon, G.J. Shiflet, J. Xu, D.H. Kim, J.F. Löffler, Formation of bulk metallic glasses and their composites, MRS Bull. 32 (2007) 624–628, doi:10.1557/mrs2007.123.

[81] C.-C. Tung, J.-W. Yeh, T. Shun, S.-K. Chen, Y.-S. Huang, H.-C. Chen, On the elemental effect of AlCoCrCuFeNi high-entropy alloy system, Mater. Lett. 61 (2007) 1–5, doi:10.1016/j.matlet.2006.03.140.

[82] C.-Y. Hsu, W.-R. Wang, W.-Y. Tang, S.-K. Chen, J.-W. Yeh, Microstructure and mechanical properties of new AlCo$_x$CrFeMo$_{0.5}$Ni high-entropy alloys, Adv. Eng. Mater. 12 (2010) 44–49, doi:10.1002/adem.200900171.

[83] F.J. Wang, Y. Zhang, Effect of Co addition on crystal structure and mechanical properties of Ti$_{0.5}$CrFeNiAlCo high entropy alloy, Mater. Sci. Eng. A 496 (2008) 214–216, doi:10.1016/j.msea.2008.05.020.

[84] C.-Y. Hsu, C.-C. Juan, W.-R. Wang, T.-S. Sheu, J.-W. Yeh, S.-K. Chen, On the superior hot hardness and softening resistance of AlCoCr$_x$FeMo$_{0.5}$Ni high-entropy alloys, Mater. Sci. Eng. A 528 (2011) 3581–3588, doi:10.1016/j.msea.2011.01.072.

[85] Y.J. Zhou, Y. Zhang, F.J. Wang, Y.L. Wang, G.L. Chen, Effect of Cu addition on the microstructure and mechanical properties of AlCoCrFeNiTi$_{0.5}$ solid-solution alloy, J. Alloys Compd. 466 (2008) 201–204, doi:10.1016/j.jallcom.2007.11.110.

[86] C.W. Chang, Microstructure and Properties of as-cast 10-1component nanostructured AlCoCrCuFeMoNiTiVZr high-entropy alloy, National Tsing Hua University, 2004.

[87] B.S. Li, Y.P. Wang, M.X. Ren, C. Yang, H.Z. Fu, Effects of Mn, Ti and V on the microstructure and properties of AlCrFeCoNiCu high entropy alloy, Mater. Sci. Eng. A 498 (2008) 482–486, doi:10.1016/j.msea.2008.08.025.

[88] J.-W. Yeh, S.-Y. Chang, Y.-D. Hong, S.-K. Chen, S.-J. Lin, Anomalous decrease in X-ray diffraction intensities of Cu–Ni–Al–Co–Cr–Fe–Si alloy systems with multi-principal elements, Mater. Chem. Phys. 103 (2007) 41–46, doi:10.1016/j.matchemphys.2007.01.003.

[89] Z. Hu, Y. Zhan, G. Zhang, J. She, C. Li, Effect of rare earth Y addition on the microstructure and mechanical properties of high entropy AlCoCrCuNiTi alloys, Mater. Des. 31 (2010) 1599–1602, doi:10.1016/j.matdes.2009.09.016.

[90] C.-Y. Hsu, T.-S. Sheu, J.-W. Yeh, S.-K. Chen, Effect of iron content on wear behavior of AlCoCrFexMo$_{0.5}$Ni high-entropy alloys, Wear 268 (2010) 653–659, doi:10.1016/j.wear.2009.10.013.

[91] J.M. Zhu, H.M. Fu, H.F. Zhang, A.M. Wang, H. Li, Z.Q. Hu, Microstructures and compressive properties of multicomponent AlCoCrFeNiMo$_x$ alloys, Mater. Sci. Eng. A 527 (2010) 6975–6979, doi:10.1016/j.msea.2010.07.028.

[92] C.-C. Juan, C.-Y. Hsu, C.-W. Tsai, W.-R. Wang, T.-S. Sheu, J.-W. Yeh, S.-K. Chen, On microstructure and mechanical performance of AlCoCrFeMo$_{0.5}$Ni$_x$ high-entropy alloys, Intermetallics 32 (2013) 401–407, doi:10.1016/j.intermet.2012.09.008.

[93] S.G. Ma, Y. Zhang, Effect of Nb addition on the microstructure and properties of AlCoCrFeNi high-entropy alloy, Mater. Sci. Eng. A 532 (2012) 480–486, doi:10.1016/j.msea.2011.10.110.

[94] Y.J. Zhou, Y. Zhang, Y.L. Wang, G.L. Chen, Solid solution alloys of AlCoCrFeNiTi$_x$ with excellent room-temperature mechanical properties, Appl. Phys. Lett. 90 (2007) 181904, doi:10.1063/1.2734517.

[95] A.K. Singh, A. Subramaniam, On the formation of disordered solid solutions in multi-component alloys, J. Alloys Compd. 587 (2014) 113–119, doi:10.1016/j.jallcom.2013.10.133.

[96] M. Chen, Y. Liu, Y. Li, X. Chen, Microstructure and mechanical properties of AlTiFeNiCuCr$_x$ high-entropy alloy with multi-principal elements, Acta Metall. Sin. 43 (2007) 1020–1024.

[97] K.-H. Cheng, C.-H. Lai, S.-J. Lin, J.-W. Yeh, Structural and mechanical properties of multi-element (AlCrMoTaTiZr)N$_x$ coatings by reactive magnetron sputtering, Thin Solid Films 519 (2011) 3185–3190, doi:10.1016/j.tsf.2010.11.034.

[98] C.-H. Lai, S.-J. Lin, J.-W. Yeh, A. Davison, Effect of substrate bias on the structure and properties of multi-element (AlCrTaTiZr)N coatings, J. Phys. D Appl. Phys. 39 (2006) 4628–4633, doi:10.1088/0022-3727/39/21/019.

[99] Y.L. Chou, J.W. Yeh, H.C. Shih, The effect of molybdenum on the corrosion behaviour of the high-entropy alloys Co$_{1.5}$CrFeNi$_{1.5}$Ti$_{0.5}$Mo$_x$ in aqueous environments, Corros. Sci. 52 (2010) 2571–2581, doi:10.1016/j.corsci.2010.04.004.

[100] Y.-J. Hsu, W.-C. Chiang, J.-K. Wu, Corrosion behavior of FeCoNiCrCu$_x$ high-entropy alloys in 3.5% sodium chloride solution, Mater. Chem. Phys. 92 (2005) 112–117, doi:10.1016/j.matchemphys.2005.01.001.

[101] X.F. Wang, Y. Zhang, Y. Qiao, G.L. Chen, Novel microstructure and properties of multicomponent CoCrCuFeNiTi$_x$ alloys, Intermetallics 15 (2007) 357–362, doi:10.1016/j.intermet.2006.08.005.

[102] T.-T. Shun, L.-Y. Chang, M.-H. Shiu, Microstructures and mechanical properties of multiprincipal component CoCrFeNiTi$_x$ alloys, Mater. Sci. Eng. A 556 (2012) 170–174, doi:10.1016/j.msea.2012.06.075.

[103] B. Ren, Z.X. Liu, D.M. Li, L. Shi, B. Cai, M.X. Wang, Effect of elemental interaction on microstructure of CuCrFeNiMn high entropy alloy system, J. Alloys Compd. 493 (2010) 148–153, doi:10.1016/j.jallcom.2009.12.183.

[104] A.K. Singh, A. Subramaniam, Thermodynamic rationalization of the microstructures of CrFeNi & CuCrFeNi alloys, Adv. Mater. Res. 585 (2012) 3–7, doi:10.4028/www.scientific.net/AMR.585.3.

[105] A. Durga, K.C. Hari Kumar, B.S. Murty, Phase formation in equiatomic high entropy alloys: CALPHAD approach and experimental studies, Trans. Indian Inst. Met. 65 (2012) 375–380, doi:10.1007/s12666-012-0138-5.

[106] O.N. Senkov, S.V. Senkova, C. Woodward, D.B. Miracle, Low-density, refractory multi-principal element alloys of the Cr–Nb–Ti–V–Zr system: Microstructure and phase analysis, Acta Mater. 61 (2013) 1545–1557, doi:10.1016/j.actamat.2012.11.032.

[107] L. Ma, L. Wang, T. Zhang, A. Inoue, Bulk glass formation of Ti-Zr-Hf-Cu-M (M=Fe, Co, Ni) alloys, Mater. Trans. 43 (2002) 277–280, doi:10.2320/matertrans.43.277.

[108] O.N. Senkov, J.M. Scott, S.V. Senkova, D.B. Miracle, C.F. Woodward, Microstructure and room temperature properties of a high-entropy TaNbHfZrTi alloy, J. Alloys Compd. 509 (2011) 6043–6048, doi:10.1016/j.jallcom.2011.02.171.

[109] Y. Zhang, X. Yang, P.K. Liaw, Alloy design and properties optimization of high-entropy alloys, JOM 64 (2012) 830–838, doi:10.1007/s11837-012-0366-5.